66-6894

LONERGAN, James Arthur, 1939-

A STUDY OF SOME PROPERTIES OF EXCITED STATES IN LIGHT NUCLEI USING ^{3}He-INDUCED REACTIONS.

University of Arizona, Ph.D., 1966
Physics, nuclear

University Microfilms, Inc., Ann Arbor, Michigan

A STUDY OF SOME PROPERTIES OF EXCITED STATES IN LIGHT NUCLEI USING ^{3}He-INDUCED REACTIONS

by

James Arthur Lonergan

A Dissertation Submitted to the Faculty of the

DEPARTMENT OF PHYSICS

In Partial Fulfillment of the Requirements
For the Degree of

DOCTOR OF PHILOSOPHY

In the Graduate College

THE UNIVERSITY OF ARIZONA

1966

THE UNIVERSITY OF ARIZONA

GRADUATE COLLEGE

I hereby recommend that this dissertation prepared under my direction by **James Arthur Lonergan**

entitled **A Study of Some Properties of Excited States in Light Nuclei Using ^{3}He-Induced Reactions**

be accepted as fulfilling the dissertation requirement of the degree of **Doctor of Philosophy**

D J Donahue — Jan 17, 1966

Dissertation Director — Date

After inspection of the dissertation, the following members of the Final Examination Committee concur in its approval and recommend its acceptance:*

D J Donahue	Jan 17, 1966
Donald Walling	Jan 17, 1966
Roy W. Emerick	17 Jan 1966
Hassan Mahmoud	1/17/66
Gerald D. Taylor	1/17/66

*This approval and acceptance is contingent on the candidate's adequate performance and defense of this dissertation at the final oral examination. The inclusion of this sheet bound into the library copy of the dissertation is evidence of satisfactory performance at the final examination.

STATEMENT BY AUTHOR

This dissertation has been submitted in partial fulfillment of requirements for an advanced degree at The University of Arizona and is deposited in the University Library to be made available to borrowers under rules of the Library.

Brief quotations from this dissertation are allowable without special permission, provided that accurate acknowledgment of source is made. Requests for permission for extended quotation from or reproduction of this manuscript in whole or in part may be granted by the head of the major department or the Dean of the Graduate College when in his judgment the proposed use of the material is in the interests of scholarship. In all other instances, however, permission must be obtained from the author.

SIGNED: James A Lonergan

ACKNOWLEDGMENT

The author is indebted to Professor Douglas J. Donahue for suggesting this research and for advice and assistance in carrying it out, and to Professor Stanley Bashkin for helpful discussions concerning this work. He also acknowledges the assistance of Mr. Matthew J. Wozniak, Jr. in taking the data and of Miss Marie A. Montaño in reducing the data and drawing many of the figures. This research was supported in part by the United States Atomic Energy Commission.

TABLE OF CONTENTS

PAGE

LIST OF TABLES vi

LIST OF FIGURES vii

ABSTRACT ix

CHAPTER

I. INTRODUCTION 1

II. THEORETICAL BASIS FOR EXPERIMENTAL PROCEDURE . . . 4
A. Doppler Shift Attenuation Method 4
B. Mixing Ratios from Angular Correlations . . 12

III. EXPERIMENTAL PROCEDURE 19
A. Angular Distributions 19
B. The Preparation of Self-Supporting Boron Foils 21
C. Excitation Functions 25
D. Mean Life Measurements 25
E. Angular Correlations 44

IV. RESULTS. 50
A. Angular Distribution 50
B. Excitation Function 55
C. Mean Lives of Excited States of ^{10}B 57
1. 1.74-MeV State 57
2. 2.15-MeV State 61
3. 3.58-MeV State 63
D. Mean Lives of Excited States of ^{14}N 66
1. 2.31-MeV State 66
2. 3.95-MeV State 69
3. 5.10-MeV State 70
E. Mixing Ratio 71

V. DISCUSSION OF RESULTS 76
A. Plane Wave Butler Theory for $(^3He,\alpha)$ Reactions 76
B. Comparison of Mean Lives to Shell Model Predictions 95

TABLE OF CONTENTS--Continued

PAGE

VI. SUMMARY AND CONCLUSION 105

APPENDIX A 108

LIST OF REFERENCES 111

LIST OF TABLES

		PAGE
I.	Stopping Power Data	27
II.	Summary of Measured Mean Lives	72
III.	Comparison of Radiative Widths with Weisskopf Estimates	97
IV.	Transition Strengths for Transitions in ^{10}B . . .	101
V.	Transition Strengths for Transitions in ^{14}N . . .	103

LIST OF FIGURES

		PAGE
1.	Stopping Power versus Velocity	9
2.	Energy Level Diagram for ^{10}B	15
3.	Pulse-Height Spectrum of α Particles at 90° to the Beam	22
4.	Pulse-Height Spectrum of α Particles for Measurements on the 2.15- and 1.74-MeV States in ^{10}B	30
5.	Pulse-Height Spectrum of α Particles for Measurements on the 3.58-MeV State in ^{10}B . . .	32
6.	Pulse-Height Spectrum of Proton for Measurements on States in ^{14}N	34
7.	Experimental Arrangement	37
8.	$M(\frac{dE}{dx})^{-1}$ vs. Velocity	42
9.	Pulse-Height Spectrum of α Particles at 0° to the Beam	46
10.	Angular Distribution for $E_{^3He}$ = 1.0 MeV	51
11.	Angular Distribution for $E_{^3He}$ = 1.8 MeV	52
12.	Angular Distribution for $E_{^3He}$ = 2.15	53
13.	Excitation Functions	56
14.	Pulse-Height γ-Ray Spectrum for Measurements on the 1.74-MeV State in ^{10}B	59
15.	Pulse-Height γ-Ray Spectrum for Measurements on the 2.15-MeV State in ^{10}B	62
16.	Pulse-Height γ-Ray Spectrum for Measurements on the 3.58-MeV State in ^{10}B	65
17.	Energy Level Diagram for ^{14}N	67

LIST OF FIGURES--Continued

PAGE

18. Pulse-Height γ-Ray Spectrum for Measurements on States in ^{14}N 68

19. Pulse-Height γ-Ray Spectrum for Angular Correlation Measurements 74

20. Schematic Diagram of Pick-up Reaction 81

21. Coordinate Diagram 83

22. Angular Distribution of α_0 89

23. Angular Distribution of α_1 91

24. Angular Distribution of α_2 92

25. Angular Distribution of α_3 94

ABSTRACT

The mean lives of the 1.74-, 2.15- and 3.58-MeV states in ^{10}B and the 2.31-MeV state in ^{14}N were measured and limits were placed on the mean lives of the 5.10- and 3.95-MeV states in ^{14}N by the Doppler-shift attenuation method. The reactions $^{11}B(^{3}He,\alpha)^{10}B$ and $^{12}C(^{3}He,p)^{14}N$ were used and the direction of the recoiling nucleus was selected by a coincidence technique. The results for the states indicated in brackets are: $^{10}B[1.74]$ $(1.90 \pm 0.30) \times 10^{-13}$ sec, $^{10}B[2.15]$ $5^{+2}_{-1} \times 10^{-12}$ sec, $^{10}B[3.58]$ $(1.75 \pm 0.70) \times 10^{-13}$ sec, $^{14}N[2.31]$ $(8.3 \pm 3.0) \times 10^{-14}$ sec, $^{14}N[3.95]$ $< 2.5 \times 10^{-14}$ sec and $^{14}N[5.10] > 2 \times 10^{-12}$ sec. The results of the measurement on ^{10}B are compared with predictions made from the independent particle model with intermediate coupling. The coupling parameter was found to have the values $1.5 < a/K < 3.0$. The results of the measurements on ^{14}N are compared with prediction made from the independent particle model with both extreme j-j coupling and L-S coupling schemes. The L-S coupling scheme was found to apply for the 2.31-MeV state and found not to apply to the 3.95-MeV state. The result of the measurement on the 5.10-MeV state is compared to predicted intensities of the three multipole radiations proposed to be present and no inconsistency with this proposal was found.

The mixing ratio of E2 to M1 multipole radiations in the transition from the 2.15-MeV state to the 0.72-MeV state in ^{10}B was measured by an angular correlation technique. The reaction $^{11}B(^{3}He,\alpha)^{10}B$ was used and the angular distribution of the γ ray was measured in coincidence with α particles emitted in the beam direction. The mixing ratio was found to be $|x| \leq 0.07$.

The angular distribution of α particles leading to the four lowest states in ^{10}B from the reaction $^{11}B(^{3}He,\alpha)^{10}B$ were measured for ^{3}He energies of 1.0, 1.8, and 2.15 MeV. The distributions were compared with predictions made from the plane-wave Butler pick-up theory which was extended to the case of $(^{3}He,\alpha)$ reactions. The comparison indicates the presence of direct interaction mechanism for the excitation of the three lowest states in ^{10}B. The α particles associated with the formation of the 2.15-MeV state in ^{10}B were symmetric about 90° in the center of mass system. The excitation functions for the formation of the five lowest states in ^{10}B by the $^{11}B(^{3}He,\alpha)^{10}B$ reaction were measured for ^{3}He energies from 1.0 MeV to 2.15 MeV.

I. INTRODUCTION

The experiments described here were performed in order to study properties of light nuclei which can be predicted by some model or mechanism. In particular, mean lives of excited states of nuclei are quantities whose numerical value can be predicted from a knowledge of the wave functions of the states. The shell model predicts the form of the wave functions and the quantum numbers which should be associated with the states. A quantum mechanical treatment of the electromagnetic interaction yields selection rules involving the quantum numbers of the states between which electromagnetic transitions occur. Applying these selection rules and using the predicted wave functions the rate at which one state decays to others by gamma ray emission can be computed. Thus, a measurement of the mean life of a state, which is inversely proportional to its decay rate, provides a check on the applicability of the model assumed.

The mean lives of three excited states of ^{10}B and three excited states of ^{14}N were measured by the Doppler-shift attenuation method and compared to shell model predictions. The measured value of the mean life of the second excited state of ^{10}B indicated that it is not strictly

a single particle state as predicted by the shell model but rather involves the excitation of several nucleons. In order to further study the collective properties of this state, the ratio of electric quadrupole radiation to magnetic dipole radiation (both of which are allowed by selection rules in the transition to the first excited state) was measured. The electric quadrupole radiation if present must be greater than predicted by single particle states in order to compete with the magnetic dipole radiations. Any such enhancement must be due to the collective properties of the initial state. Thus, a determination of the ratio of E2 to M1 multipole radiations provides a measure of the collective properties of the state. A technique which compares the angular distribution of gamma radiation from two different decay modes of the state was used to measure this mixing ratio.

The excited states studied in these experiments were all produced by either the reaction $^{11}B(^{3}He,\alpha)^{10}B$ or $^{12}C(^{3}He,p)^{14}N$. In order to more efficiently use the Doppler-shift method of measuring mean lives, it was necessary to know the angular distribution of the low-mass particles emitted in the above reactions. A complete study of the angular distribution of alpha particles from the formation of the ground and first three excited states of ^{10}B was made. The results indicated the presence of a direct reaction

mechanism. The Butler plane-wave theory was extended to this case and attempts were made to fit the measured distributions.

II. THEORETICAL BASIS FOR EXPERIMENTAL PROCEDURE

A. Doppler-Shift Attenuation Method

The mean lives of excited nuclear states are usually less than 10^{-8} seconds and greater than 10^{-18} seconds. There are many techniques for measuring mean lives in this range and these can be classified into two categories according to the quantity actually measured. Mean lives greater than about 2×10^{-14} sec can be measured directly. That is, some timing technique can be used to measure the rate of decay. A mean life less than about 5×10^{-13} sec can be obtained from a measurement of the width of the state since this width is inversely proportional to the mean life of the state. The Doppler-shift technique falls in the first category since it measures mean lives directly by relating the attenuation of the Doppler shift with the slowing-down time associated with the material used. The range of applicability of this method depends somewhat on the particular experimental conditions, but is about 2×10^{-12} to 2×10^{-14} sec. This is the only way mean lives can be directly measured in this range, although they can be obtained indirectly through the width measurement techniques which overlap part of this range. This overlap provides an independent check on the results lying in the overlapping region.

The Doppler-shift technique has been used in various forms by other workers.[1-3] The form which was used in these experiments was suggested by Devons.[1] However, the method of analyzing the measured shift to obtain the mean lives has been extended. The outgoing particle B from the reaction A(x,y)B will recoil with a velocity dependent on the incident energy of the incoming particle, x, the Q-value of the reaction and the recoil direction of particle, y. If the target material is supported by a thick backing the recoiling particle will slow down from that initial velocity in a manner which can be related to the stopping power of the backing material.

The energy of a gamma ray emitted by a moving nucleus is given to first order in v/c by

$$E = E_0[1 + \frac{v}{c} \cos \theta], \qquad (1)$$

where E is the observed energy in the laboratory reference frame, E_0 is the energy of the γ ray in the rest frame of the nucleus, v/c is the ratio of the speed of the recoiling nucleus to the speed of light, and θ is the angle between the direction of observation and the direction of motion of the nucleus. Since $v/c \approx 10^{-2}$, the change in energy due to the Doppler effect is a few percent of E_0. Thus very good energy resolution is required in order to measure this change directly. However, if the gamma radiation is

observed at two different angles, one observes a shift in energy given by

$$\Delta E = E_1 - E_2 = \frac{v}{c} (\cos \theta_1 - \cos \theta_2), \qquad (2)$$

where indices 1 and 2 refer to the two positions of observation. If these positions are chosen to be along the direction of recoil ($\theta_1 = 0°$) and at 180° to that direction ($\theta_2 = 180°$), the maximum shift is observed. In this manner, the ratio v/c can be determined without having to know the energy calibration precisely.

In the experiments performed here the Q-values of the reactions were much greater than the energy of the incident particle. When this is the case the velocity of the recoiling nucleus, B, will be almost as large when moving in the backward direction relative to the incident particle as when moving in the forward direction. That is, as Q becomes much greater than the energy of the incident particle the velocity distribution becomes isotropic about the target. Thus, if the gamma radiation from decaying nuclei recoiling in all directions is observed, the energies of these γ rays will be symmetrically broadened about the zero velocity value and no shift can be measured. For this reason it was necessary to observe only those γ rays which were in coincidence with particles, y, proceeding in a given direction. By fixing the recoil direction of the particle,

y, the direction of motion and initial speed of recoiling particle, B, are uniquely determined.

In the actual experiment many γ rays were observed. The velocity at which they were emitted varies from the initial value (fixed by the kinematics) to zero because the decay of the state is exponential in time. However, the peak of the γ-ray energy distribution seen by a NaI detector will occur at, or very close to, the energy associated with the average velocity (see Appendix A) defined by the equation

$$\bar{v} = \frac{1}{\tau} \int_0^\infty v(t)\, e^{-t/\tau}\, dt \,, \qquad (3)$$

where τ is the mean life of the state. In order to determine the mean life from the measured value of the average velocity the integration indicated in equation (3) must be performed.

In general, the function $v(t)$ can not be accurately expressed in an analytic form. It is necessary to make use of some empirical values of the stopping power, $\frac{dE}{dx}$, for the material in which the nucleus slows down. The relationship between velocity and $\frac{dE}{dx}$ is given by

$$\frac{dE}{dx} = -m \frac{dv}{dt} \qquad (4)$$

where m is the mass of the moving ion. In the velocity region in which these experiments were performed, i.e.,

$v/c \leq 2.5 \times 10^{-2}$, approximations can be made about the dependence of stopping power on velocity. In Figure 1, measured values of stopping power are plotted versus velocity for the case of boron ions moving in copper. If the stopping power in the region from $v = 0$ to $v = v'$ is approximated by assuming $dE/dx \propto v$ and if in the region from $v = v'$ to $v = v_o$, where v_o is the initial velocity of the moving ion, the stopping power is approximated by assuming $dE/dx =$ constant, then a reasonable and simple analytic dependence of dE/dx on v is obtained (solid line). It should be noted that the reasonableness of this approximation results in part from the fact that the data for dE/dx are uncertain by 10%. Therefore, if it is assumed that $dE/dx = \frac{mv_o}{\alpha}$, where this form of the constant was chosen for convenience, then

$$\frac{dE}{dx} = -m \frac{dv}{dt} = \frac{mv_o}{\alpha}, \qquad (5)$$

where m is the mass of the moving ion and v_o is its initial speed. Apparently α, a constant which is determined from stopping power data, has the units of time. Integrating equation (5) yields an expression for speed as a function of time

$$v = v_o[1 - t/\alpha], \quad (v' < v \leq v_o). \qquad (6)$$

Here v' is the lowest speed for which the approximation applies. At lower speeds the stopping power approaches a

Fig. 1. Stopping Power versus Velocity. The shaded area corresponds to values that are consistant with experimental data as compiled by Northcliff.[11] The solid line is the analytic fit used in the analysis.

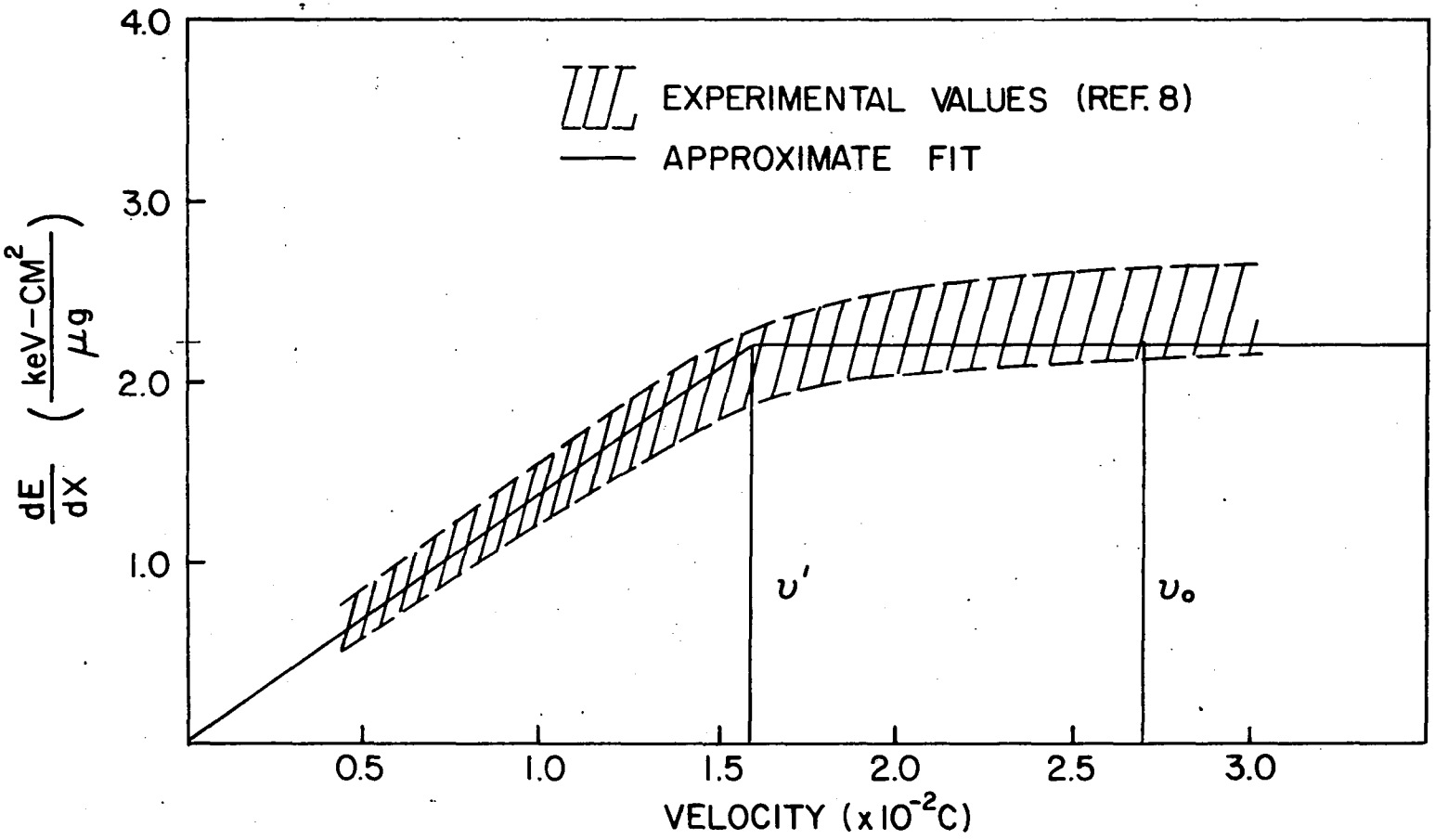
EXPERIMENTAL VALUES (REF. 8)
APPROXIMATE FIT
4.0
3.0
2.0
1.0
dE/dX (keV-CM²/μg)
0.5
1.0
1.5
2.0
2.5
3.0
VELOCITY (x10⁻²C)
υ'
υ₀

linear dependence on velocity. In this region the stopping power is assumed to have the form

$$\frac{dE}{dx} = -m\frac{dv}{dt} = \frac{m}{\beta}v, \qquad (7)$$

where again the form of the proportionality constant, m/β, is chosen for convenience. Here β has the units of time and is determined from the stopping power data. Integrating equation (7) yields another expression for speed as a function of time

$$v = v_1 e^{-t/\beta} \qquad (0 \leq v \leq v') \qquad (8)$$

which is assumed to approximate the true situation for speeds less than v' defined above. Here v_1 is a constant of integration which is chosen so that the speed, v', will occur for the same time, t_1, in both expressions, thus insuring continuity of v(t) between the two expressions. The value of v_1 which satifies this condition is

$$v_1 = v' e^{t_1/\beta} = v' \exp\left[\frac{\alpha}{\beta}\left(1 - \frac{v'}{v_o}\right)\right], \qquad (9)$$

where t_1 is expressed in terms of v' through equation (6). The method used to determine α, β and v' will be described in the section on experimental procedure.

An expression for the average velocity defined by equation (3) is obtained by first substituting the expression

for v(t) for the high speed region (equation (6)) and performing the indicated integration from v_o to v'. Then the expression for v(t) for the low speed region (equation (8)) is substituted into equation (3) and the integration performed from v' to 0. The results of these two integrations are summed to give the following expression for the average velocity in terms of the mean life, τ, and the stopping power parameters

$$\bar{v} = v_o\left\{\left[\frac{\tau}{\alpha} - \frac{v'}{v_o}\left(\frac{\tau}{\beta + \tau}\right)\right] \exp\left[-\frac{\alpha}{\tau}\left(1 - \frac{v'}{v_o}\right)\right] + 1 - \frac{\tau}{\alpha}\right\}. \quad (10)$$

Therefore, the attenuated Doppler-shift method consists in obtaining the average velocity from the measured Doppler shift and relating that velocity to the mean life through equation (10).

The method of analysis described above differs from methods used by others[1,3] in that an analytic function for v(t) has been extended into the velocity region where dE/dx is constant. Heretofore, when sufficient energy was available in order to obtain velocities greater than about 5×10^8 cm/sec, the analysis was made by numerical methods on computers.[2] In principle, the numerical methods are more accurate. However, in practice the knowledge of stopping power is so uncertain that little is lost by making these approximations which lead to equation (10).

At low velocities the stopping ceases to be dominated by electronic interactions as it is for higher velocities. That is, for velocities less than about 10^8 cm/sec some collisions with the atoms of the stopping material occur which may change the direction of the recoiling particle. Atomic scattering will have the effect of making the average velocity of the ions entering this region drop rapidly to zero, or equivalently the stopping power becomes infinite. Litherland et al.[2] have shown that if the worst practical case is assumed, that is, if dE/dx becomes infinite for $v < 10^8$ cm/sec, then the error incurred by assuming $dE/dx \propto v$ down to $v = 0$ is less than 1% of the maximum Doppler shift. Since Doppler shifts are seldom measured to better than about 5%, the effect of atomic scattering can usually be neglected.

B. Mixing Ratios from Angular Correlations

In this section a method is described for measuring the mixing ratio in the γ-ray decay of one state to another. That is, if in the decay of one state to another two multipolarities are allowed by the selection rules, the mixing ratio is defined as the ratio of matrix elements of the two different multipole radiations in the transition. There are several ways in which mixing ratios can be determined from angular correlation experiments, and only the details of the

method employed here will be described. A general treatment of the problem is given by Litherland and Ferguson[4] who developed the technique. A measurement similar to the one described here was made by Warburton et al.[5] who particularized the formalism to the situation which appears in the present measurements.

The technique is to measure the angular distributions of two separate γ-ray transitions from the same state and compare the results. If one of the transitions is a pure multipole and the other a mixture of two multipoles, then the difference in the two distributions can be expressed as a function of the mixing ratio. When a state of definite angular momentum and parity is formed by some process, the direction of its angular momentum is restricted by the conservation of angular momentum. Such a state bears no other evidence of its mode of formation. Furthermore, it has been shown[6] that if the restrictions on the direction of the angular momentum of the excited state are such that an axis of symmetry is defined, then the decay of the state will be symmetric about a plane perpendicular to this axis. This is a result of the state having definite parity regardless of what the parity is. Therefore, the angular distribution of decay products relative to the axis of symmetry can be expanded in a series of even Legendre polynomials as follows

$$W(\theta) = \sum_{n=0}^{\infty} A_{2n} P_{2n} (\cos \theta). \qquad (11)$$

The coefficients A_{2n} will depend on the particular circumstances of the case in question.

In the present case the mixing ratio of E2 to M1 multipole radiations in the transition from the 2.15-MeV state to the 0.72-MeV state in ^{10}B was measured. A level diagram for this nucleus along with the known spin, parity and isotopic spin assignments is shown in Figure 2. The possible decays of the excited states are indicated by the arrows which are labeled with the branching ratios and possible multipolarities. The 2.15-MeV state of ^{10}B was formed from the reaction $^{11}B(^{3}He,\alpha)^{10}B^{*}$. If the α particle from the reaction is observed along the beam axis the restrictions on angular momentum of the excited states of B^{10} will be such as to make the beam axis an axis of symmetry. Thus, the γ radiation from the decay of the 2.15-MeV state will be symmetrically distributed according to equation (11), where θ is the angle between the incident beam and the outgoing γ ray. The reason the beam direction is not sufficient to define an axis of symmetry is that no assumptions can be made about the definiteness of the spin and parity of the $^{11}B + ^{3}He$ system. However, any uncertainty about the symmetry properties of the beam direction is removed if the α

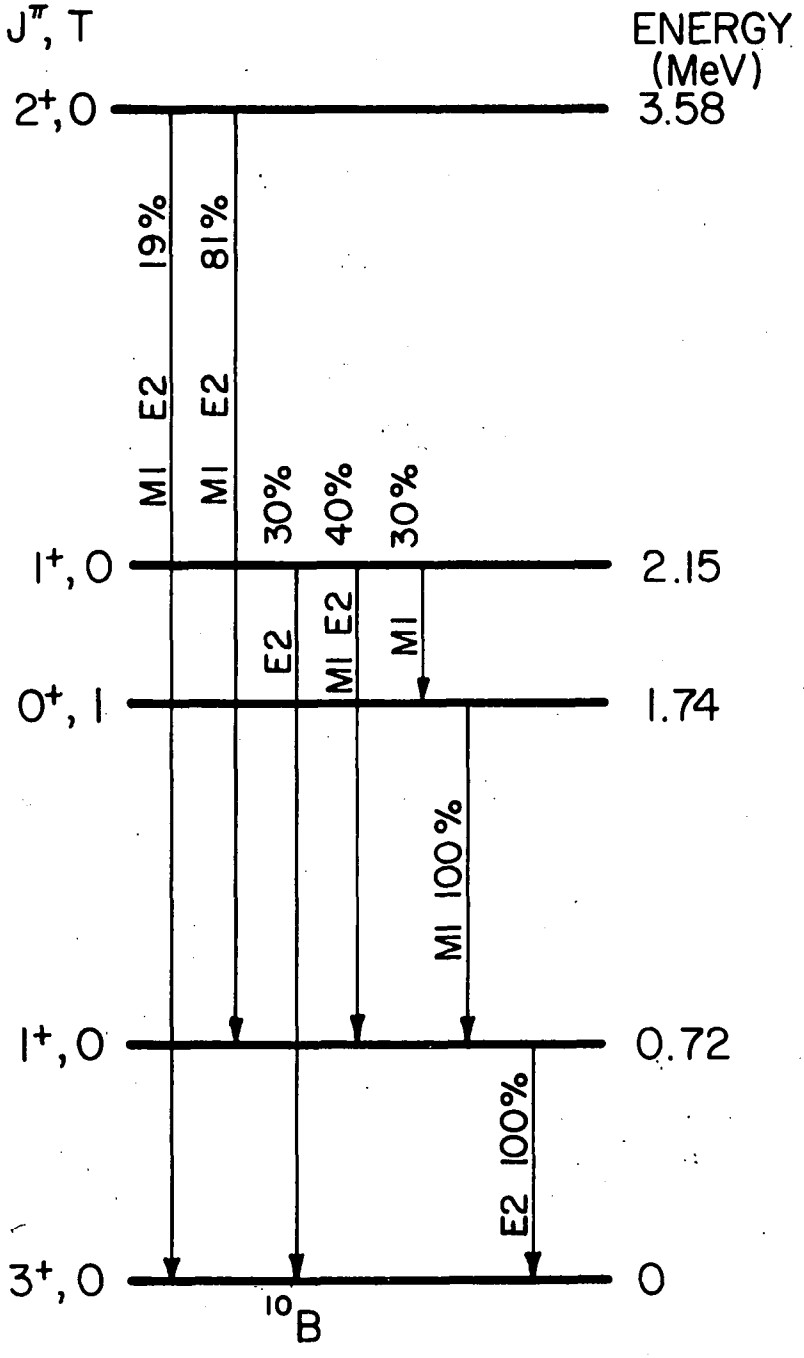

Fig. 2. Energy Level Diagram for ^{10}B.

particle is emitted along this axis since the excited state of ^{10}B has definite spin and parity.

The values of A_{2n} in equation (11) for a given transition depend on the initial and final state spins and parities, the population of the magnetic substates in the initial state and the multipole mixing, if any is possible. A general expression for the distribution is given by Litherland and Ferguson[4] in their equation (23). This equation was obtained by averaging over all possible intermediate states which lead to the state being studied. The angular momentum restrictions on all these intermediate states are systematically accounted for by the Racah algebra. Warburton et al.[5] have reduced this equation for the case where the initial state has spin and parity 1^+ and the final states have spins and parities 0^+ and 1^+. Their result for the $1^+ \rightarrow 0^+$ pure M1 transition is

$$W(\theta) = 1 + F_2(1)P_2(\cos\theta), \qquad (12)$$

where $F_2(1)$ is a function of the populations of the magnetic substates. Their result for the $1^+ \rightarrow 1^+$ transition where both M1 and E2 multipole radiations are possible is

$$W(\theta) = [1 - \tfrac{1}{2}F_2(1)f(x)P_2(\cos\theta)], \qquad (13)$$

where $F_2(1)$ is the same as for equation (12). Here f(x) is a function of the mixing ratio, x, and is given by

$$f(x) = \frac{1 - 6x + x^2}{x^2 + 1} , \qquad (14)$$

where the mixing ratio, x, is formally defined by

$$x = \frac{\langle b|L + 1|a \rangle}{\langle b|L|a \rangle} \qquad (15)$$

Here a and b indicate the initial and final states between which multipole transitions of order L and L + 1 are possible. The fact that both distributions depend on the populations of the magnetic substates in the same way through $F_2(1)$ is a result of the fact that only one such population is unknown. The 2.15-MeV state has quantum numbers 1^+ and thus can have magnetic quantum numbers $m_j = \pm 1, 0$; but the axial symmetry requires that the populations, $P(m_j)$, satisfy the following relation

$$P(m_j) = P(-m_j) . \qquad (16)$$

Also these populations are subject to the normalization condition

$$\sum_{mj} P(m_j) = 1 . \qquad (17)$$

Therefore, there is only one unknown among the three populations.

In the present case the distributions of the pure M1 transition from the 2.15-MeV state to the 1.74-MeV state was used to determine $F_2(1)$. A value for f(x) was then obtained from the angular distribution of the 1.43-MeV γ rays. The mixing ratio was determined from f(x) through equation (14).

III. EXPERIMENTAL PROCEDURE

A. Angular Distribution

The angular distributions of alpha particles from the formation of the first four states in ^{10}B produced by the reaction $^{11}B(^{3}He,\alpha)^{10}B$ were measured. These measurements consisted in directing a beam of ^{3}He particles at a thin foil of ^{11}B and then observing the number of outgoing particles as a function of their direction relative to the beam. This was done for three different energies of incident ^{3}He particles, 1.00 MeV, 1.80 MeV and 2.15 MeV. Since the beam current fluctuates it was necessary to standardize the number of incident particles by observing simultaneously the number of outgoing particles at a fixed angle.

The target chamber used for this experiment was 12" in diameter and about 4" high. The beam was produced by the 2-MeV Van de Graaff accelerator in the Physics Department of this University. This beam was deflected into the target chamber by an analyzing magnet and then collimated at the entrance to the target chamber. The collimating slit was circular with a diameter of 3/16" and was made from 10-mil tantalum. The collimated beam was then incident on a thin foil which was $\frac{1}{4}$" in diameter and located at the center of

the target chamber. The method used to prepare thin self-supporting boron foils will be discussed separately below.

The outgoing particles were observed by two detectors, one was mounted on a rotating arm, the other was fixed at 135° to the beam direction. The fixed detector was used to monitor the beam current. The fixed silicon surface barrier detector used was connected to a bias amplifier. The bias was set so that it passed only those pulses which corresponded to maximum energy loss by protons in the detector. These pulses were chosen because they were well separated from smaller pulses and because they were produced by reactions of the beam with the boron only and not with contaminates like carbon which are built up by bombardment. In particular protons from the reaction $^{11}B(^{3}He,p)^{13}C$ forming the four lowest states in ^{13}C contributed most of the pulses. The remaining pulses were produced by deuterons from the reaction $^{11}B(^{3}He,d)^{12}C$ to the ground state in ^{12}C. These pulses were counted by a scaler and the sum was used to normalize the α-particle yields at each angle.

The rotating detector was also a silicon surface barrier detector and had a sensitive area of 25 mm^2. It could be rotated about an axis through the target with the detector face $5\frac{1}{4}$" from the center of the target. The angle subtended by the detector surface at the target was 5°. The detector was covered with 6.33 mm of Mylar for angles of observation greater than 50° to the beam direction and by

12.6 mm of Mylar for smaller angles. This was necessary in order to prevent elastically scattered ^{3}He particles from entering the detector since they are sufficiently numerous to exceed the time resolution of the electronic equipment. The pulses from the detector were amplified and stored in a multichannel analyzer. Spectra were taken at 5° intervals from about 7° to about 170°.

The α-particle yield was determined from the spectra by adding the number of pulses corresponding to the α-particle groups concerned. The spectrum which was observed at 90° to the beam for an incident ^{3}He energy of 2.15-MeV is shown in Figure 3. The peaks corresponding to the α-particle groups are labeled by the state formed in the (^{3}He,α) reaction. The oxygen peak is the result of a contamination on the target. The background, especially evident under peaks from low energy protons, is produced by a continuum of α particles from the breakup of ^{13}N formed by the reaction $^{11}B(^{3}He,n)^{13}N$ into (3α + p). Corrections for the background were made by estimating the continuum (dashed line in Figure 3) and subtracting the contribution of the continuum from the total counts in the peak.

B. The Preparation of Self-Supporting Boron Foils

Thin foils of ^{11}B were prepared by evaporation techniques from boron powder enriched to 98% ^{11}B. The powder

Fig. 3. Pulse-Height Spectrum of α Particles at 90° to the Beam. The peaks are labeled by the state in ^{10}B formed in the $^{11}B(^{3}He,\alpha)^{10}B$ reaction. The oxygen peak is the result of target contamination. The dashed line indicates the estimated background due to the $(3\alpha + p)$ breakup of ^{13}N.

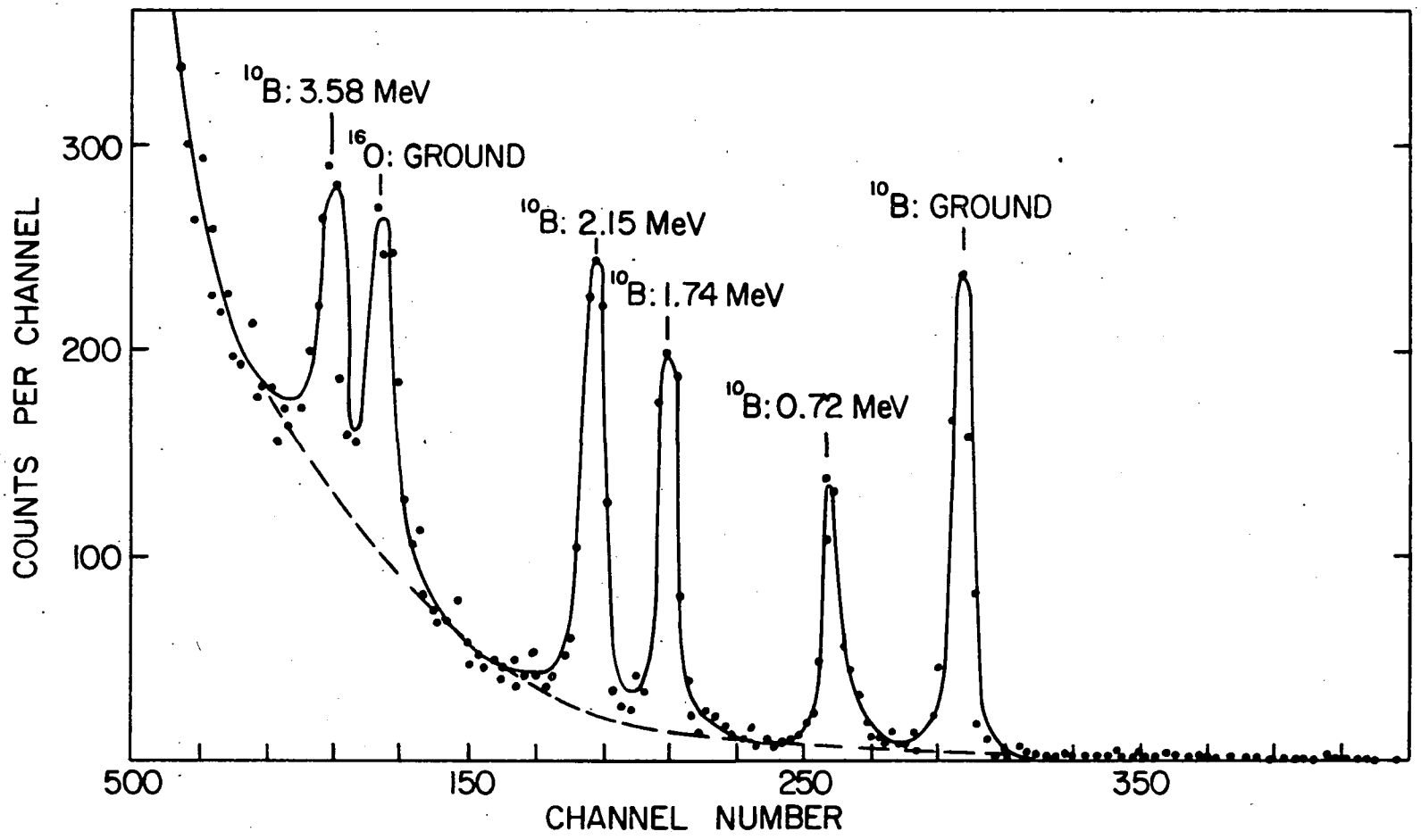
^{10}B: 3.58 MeV
^{16}O: GROUND
^{10}B: 2.15 MeV
^{10}B: 1.74 MeV
^{10}B: 0.72 MeV
^{10}B: GROUND
COUNTS PER CHANNEL
300
200
100
500
150
250
350
CHANNEL NUMBER

was placed in a tantalum boat mounted in a vacuum chamber. Glass slides were cleaned and then coated with detergent. The soap film was polished until its presence was not detectable to the eye. These slides were then placed in the vacuum chamber with the coated side facing the boat. The chamber was evacuated to a pressure of about 2×10^{-6} millimeters of mercury. Current was passed through the boat, gradually heating it to the melting point of boron. A shield was placed over the boat while it was being heated in order to keep impurities, which boil off at lower temperatures, from contaminating the slides. When the boron was hot enough it wets the boat. The shield was then removed and the slides became coated with the evaporated boron. Usually the slides were exposed for only a few seconds in order to reduce their heating, since boron has a tendency to blister. Also by applying the boron in bursts, some control over the thickness can be obtained. Nevertheless, many attempts were made before the proper thickness was obtained; since, if the foil is too thin it will not support itself and if it is too thick severe crystallization causes it to break up into very small unusable pieces.

Once a film of the proper thickness was evaporated onto the slide, a procedure first outlined by Dearnely[7] was used to remove the foil from the slide. First the film was divided into sections of the size required for the experiment

by simply scratching it with a sharp instrument. Then the slide was slowly and smoothly immersed in a solution of distilled water and several drops of wetting agent which decreased the surface tension. It was found that an angle of about 30° between the slide and the surface of the water worked best. As the soap came in contact with the water it dissolves so that the film floated off onto the surface of the water.

The foils were mounted on the frames which were copper sheets with a $\frac{1}{4}$" hole drilled through them. Care was taken to remove all rough edges which could readily puncture the foils. Mounting was accomplished by immersing the frame completely and then drawing it to the surface directly under the foil. As the frame emerges from the bath the foil will adhere to it. Until the foil drys it is very weak and the slightest air current or jar will spoil it. After it drys it becomes more durable although care still must be exercised when handling it. It was found that greater strength and thicker foils could be obtained if the foils were picked up so that they overlapped both sides of the hole. The thickness of the foils was roughly determined, by weighing, to be about 20 $\mu g/cm^2$. The inaccuracy of this method of determining thickness is principally due to the presences of tantalum which may be evaporated along with the boron.

C. Excitation Functions

The excitation function, that is the cross section as a function of incident energy, was measured for the formation of the five lowest states in ^{10}B by the reaction $^{11}B(^{3}He,\alpha)^{10}B$. These measurements were made by observing, at 90° to the beam, the number of α particles from the formation of these states over a range of ^{3}He energies. The targets were thin self-supporting foils of ^{11}B described in section III B. The beam current was monitored by collecting the charge in a Faraday cup along the beam axis behind the foil. The charge was then recorded by a current integrator. The target chamber and α-particle detection system were the same as those described in section III A for the angular distribution measurements. The energy was varied from 1.00 MeV to 2.00 MeV in increments of 100 keV and then from 2.00 MeV to 2.15 MeV in increments of 50 keV. The data were recorded in a multichannel analyzer. The procedure for analyzing the data was the same as that described in section III A.

D. Mean Life Measurements

The mean lives of three states in ^{10}B were measured using the reaction $^{11}B(^{3}He,\alpha)^{10}B$ and the mean lives of three states in ^{14}N were measured using the reaction $^{12}C(^{3}He,p)^{14}N$.

The targets in all cases were prepared by evaporating a thin film onto a thick backing material.

The choice of backing material depends on the order of magnitude of the mean life. If the state is short-lived, that is, its mean life is less than 10^{-13} sec, a fast stopping material with high stopping power should be used so that the mean final velocity is measurably less than the initial velocity. Similarly, if the state is relatively long-lived, that is, if the mean life is greater than about 10^{-13} sec, a material with a small stopping power is preferred in order that the mean final velocity be measurably different from zero. The stopping power referred to here and in equation (4) has units of energy per unit length and is the product of the density of the material times its stopping power in units of energy length-squared per unit mass. Table I lists stopping power data in both units as well as the densities for several stopping materials. These data were obtained for 3-MeV boron ions by Porat et al.[8,9] In the experiments described here copper and magnesium were used. It was found that these two materials while having extreme values of stopping power had overlapping regions of applicability and were therefore sufficient for all the experiments.

The outgoing alpha particles or protons were detected by a silicon surface barrier detector with a

TABLE I.

Stopping Power Data

Stopping Material	$\frac{dE}{dx}$[a] $(\frac{kev\text{-}cm^2}{\mu g})$	Density[b] (g/cc)	$\frac{dE}{dx}$ $(\frac{kev}{\mu})$
Carbon	5.2	2.25	11.7
Aluminum	3.8	2.7	10.4
Nickel	2.4	8.8	21.0
Silver	1.8	10.5	18.9
Gold	1.0	19.3	19.3
Magnesium	4.0	1.7	6.9
Copper	2.3	8.9	20.6

[a]These data were obtained for boron ions at 3.0 MeV by Porat et al. (Reference 8,9).

[b]These data were obtained from the Handbook of Physics and Chemistry (Reference 16).

sensitive area of 200 mm^2 placed 1.5 cm from the beam. A $\frac{1}{2}$-mil Mylar cover over the detector prevented elastically scattered ^3He nuclei from being counted. For the mean life measurement of the 1.74-MeV state in ^{10}B the α-particle detector was placed at 90° to the beam. Angular distribution measurements indicated a maximum in the number of α particles emitted near this angle. The angular distribution of the α particles from the formation of the excited state, at 2.15 MeV, showed a minimum near 90° to the beam. So at 90° the ratio of α particles from the formation of the 2.15-MeV state to α particles from the formation of the 1.74-MeV state was a minimum. This condition is preferred because these two groups were not resolved in the α-particle spectrum. The reason for this is that the energy of these α particles varies with angle so that the use of a large detector resulted in sufficient spread in energies of the α particles observed for the groups to overlap. When a coincidence criterion was applied to the pulses from the α-particle detector, it was not possible to completely discriminate against all the α particles from the formation of the 2.15-MeV state and yet accept an appreciable number of α particles from the formation of the 1.74-MeV state. As is indicated in Figure 1, the 2.15-MeV state decays to the 1.74-MeV state 30% of the time. Therefore, 30% of the α particles from the formation of the higher energy state will be in coincidence with the subsequent decay of the 1.74-MeV state. The mean

life of the 2.15-MeV state is long compared to that of the 1.74-MeV state, although much shorter than the resolving time of the coincidence circuit. The nuclei in the 1.74-MeV state which were populated by cascades from the 2.15-MeV state will then be moving much slower on the average than those populated directly, or equivalently, the zero time is shifted by an amount about equal to the mean life of the 2.15-MeV state. This could lead to an incorrect measurement so that the population of the 2.15-MeV state must be minimized by discriminating the α particles or by judiciously choosing the position of the α-particle detector.

The criterion used in the selection of the α particles for the measurement on the 1.74-MeV state is indicated by C_1 in Figure 4. This figure shows an α-particle spectrum observed by the solid state detector. The peaks are labeled with the state whose formation is associated with the group forming the peak. This criterion was applied by using a lower level discriminator on the detector pulse amplifier. The fact that α particles from the formation of lower states in ^{10}B opened the coincidence gate just increased the chance coincidence rate. Also in Figure 4 is shown the criterion, C_2, used to select α particles for the measurements on the 2.15-MeV state. In this measurement there was no complication from cascade populations. However, the fact that α particles from lower states opened the

Fig. 4. Pulse-Height Spectrum of α Particles for Measurements on the 2.15- and 1.74-MeV States in ^{10}B. The reaction $^{11}B(^{3}He,\alpha)^{10}B$ with $E_{^{3}He} = 1.8$ was used to form these states. The detector was covered by $\frac{1}{2}$ mil of Mylar. C_1 and C_2 are acceptance criteria for the coincidence pulses used in these measurements.

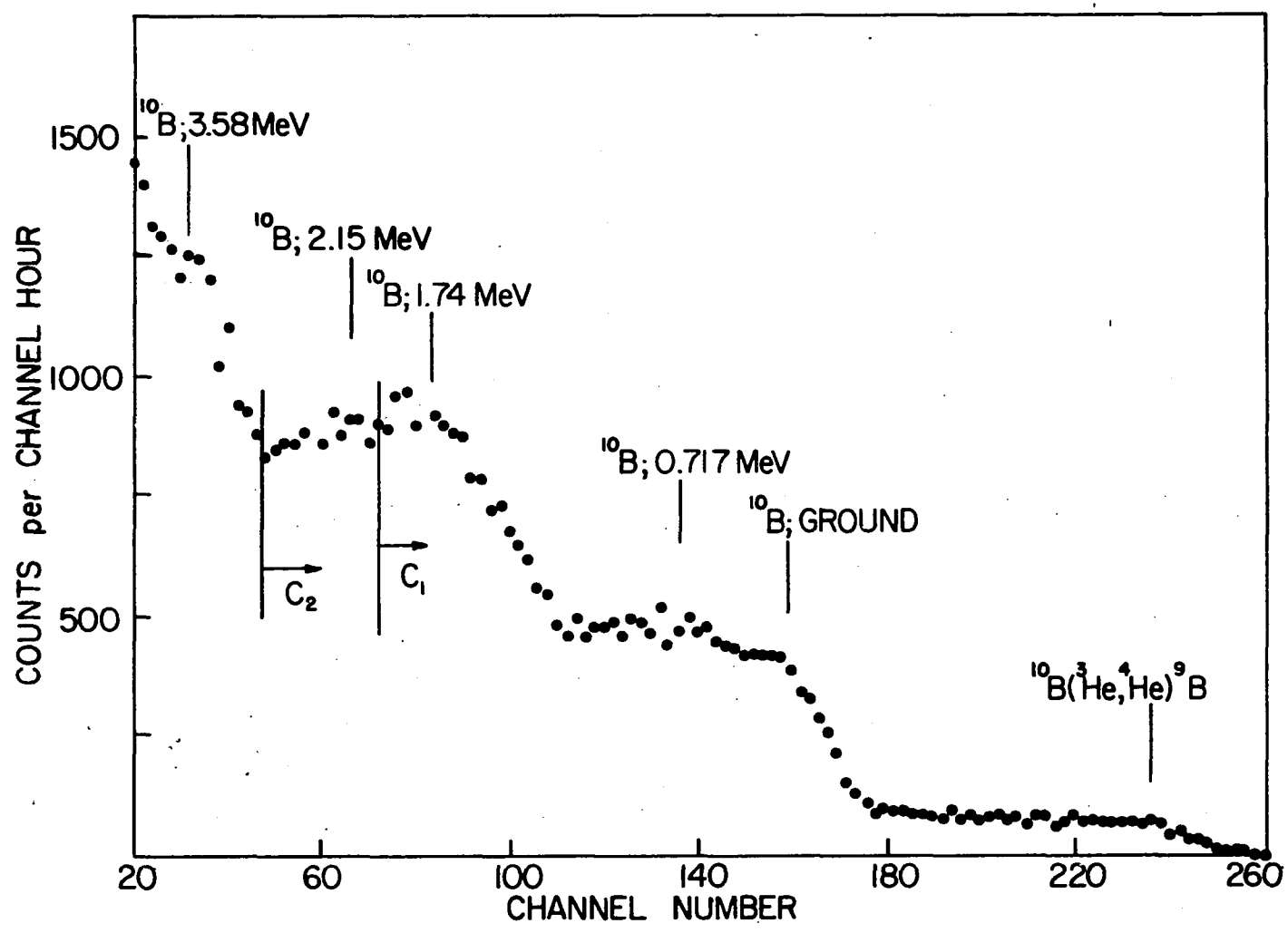
^{10}B;3.58MeV
^{10}B; 2.15 MeV
^{10}B; 1.74 MeV
^{10}B; 0.717 MeV
^{10}B; GROUND
^{10}B(^{3}He,^{4}He)^{9}B
C_2
C_1
COUNTS per CHANNEL HOUR
1500
1000
500
20
60
100
140
180
220
260
CHANNEL NUMBER

coincidence gate seriously increased the chance coincidence rate. In order to keep the ratio of chance coincidence to total coincidences down to 1:3 it was necessary to limit the beam current to about 0.5μa. The ratio of chance to true coincidences was checked by comparing the γ-ray spectrum observed under experimental conditions with the spectrum observed when a delay was placed in the coincidence leg sufficient in magnitude to insure the absence of time coincidence.

For measurements on the 3.58-MeV state a different arrangement had to be used. The α-particle group leading to the formation of this state is low enough in energy that it is indistinguishable from the peak resulting from the maximum energy lost by protons in the detector used for the measurements on the two lower states. That detector had a depletion depth of 500 micron. A thinner detector was used with a depletion depth of 60 microns for the measurement on the 3.58-MeV state. It was also necessary to increase the beam energy from 1.8 MeV to 2.0 MeV, thereby increasing the energy of all the alpha particles. Finally, it was necessary to improve the resolution by moving the detector away from the target so that its sensitive face was now 5 cm from the center of the target. With the detector located at 90° to the beam the spectrum displayed in Figure 5 was observed. The α-particle groups from the formation of the ground and

Fig. 5. Pulse-Height Spectrum of α Particles for Measurements on the 3.58-MeV State in ^{10}B. The reaction $^{11}B(^{3}He,\alpha)^{10}B$ with $E_{^{3}He} = 2.0$ MeV was used to form this state. The detector was covered by $\frac{1}{2}$ mil of Mylar. The region, GATE, indicates the criterion for coincidence pulses used in these measurements.

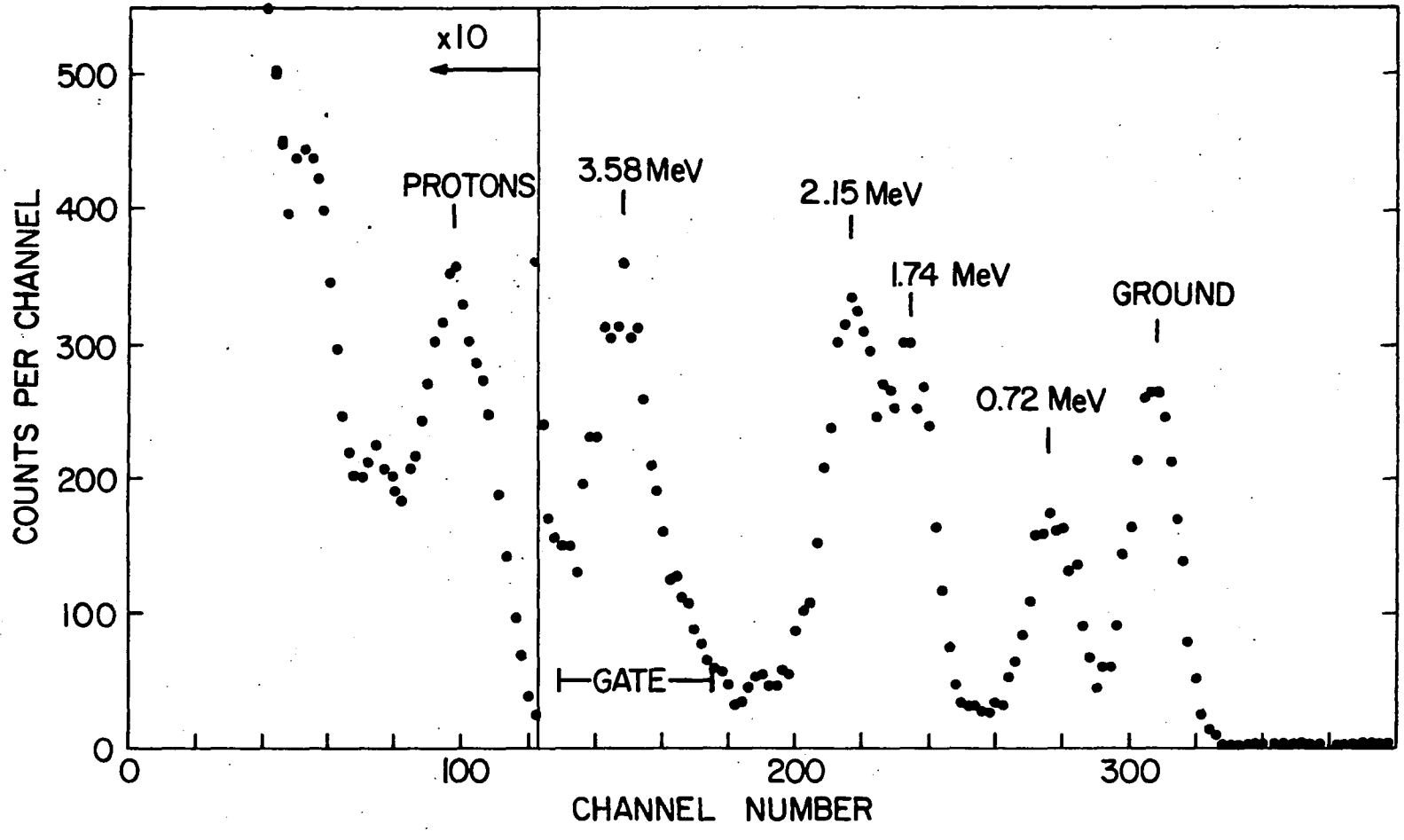
x10
PROTONS
3.58 MeV
2.15 MeV
1.74 MeV
GROUND
0.72 MeV
GATE
COUNTS PER CHANNEL
CHANNEL NUMBER
0
100
200
300
400
500
0
100
200
300

first four excited states are labeled by the state formed. The protons which are produced by (^{3}He,p) reactions on ^{11}B and carbon contamination leave a fixed energy as they pass through the counter and the associated peak is shown to a reduced scale in the figure. The group, from the formation of the 3.58-MeV states, was selected in this case by a single channel analyzer. The upper and lower discriminators were set to pass only those pulses lying in the GATE region indicated on the figure. The use of the single channel analyzer greatly reduced the number of chance coincidences.

The same procedure used with the 1.74- and 2.15-MeV states in ^{10}B was used in the measurements of the mean lives of the 2.31- and 3.95-MeV states in ^{14}N. In this case the reaction ^{12}C(^{3}He,p)^{14}N was produced with 2.0-MeV ^{3}He ions and a carbon target evaporated on a copper backing. The protons were detected with a silicon surface barrier detector which had a sensitive area of 200 mm^{2} and a depletion depth of 500 microns. It was located at 110° to the beam and its surface was 1.5 cm from the center of the target. The peaks in the spectrum observed were broadened because of the large angle of observation. However, the separations of states in this case were wide enough that the proton groups were clearly resolved. The spectrum obtained is shown in Figure 6, where the proton groups are labeled according to the state with whose formation they are associated. A lower

Fig. 6. Pulse-Height Spectrum of Protons for Measurements on States in ^{14}N. These protons result from the reaction $^{12}C(^{3}He,p)^{14}N$ with $E_{^{3}He}$ = 2.0 MeV. The detector was covered with 6 mg/cm^2 of aluminum. C_1 and C_2 are acceptance criteria for the coincidence pulses in the measurements of the 2.31-MeV state and the 3.95-MeV states, respectively.

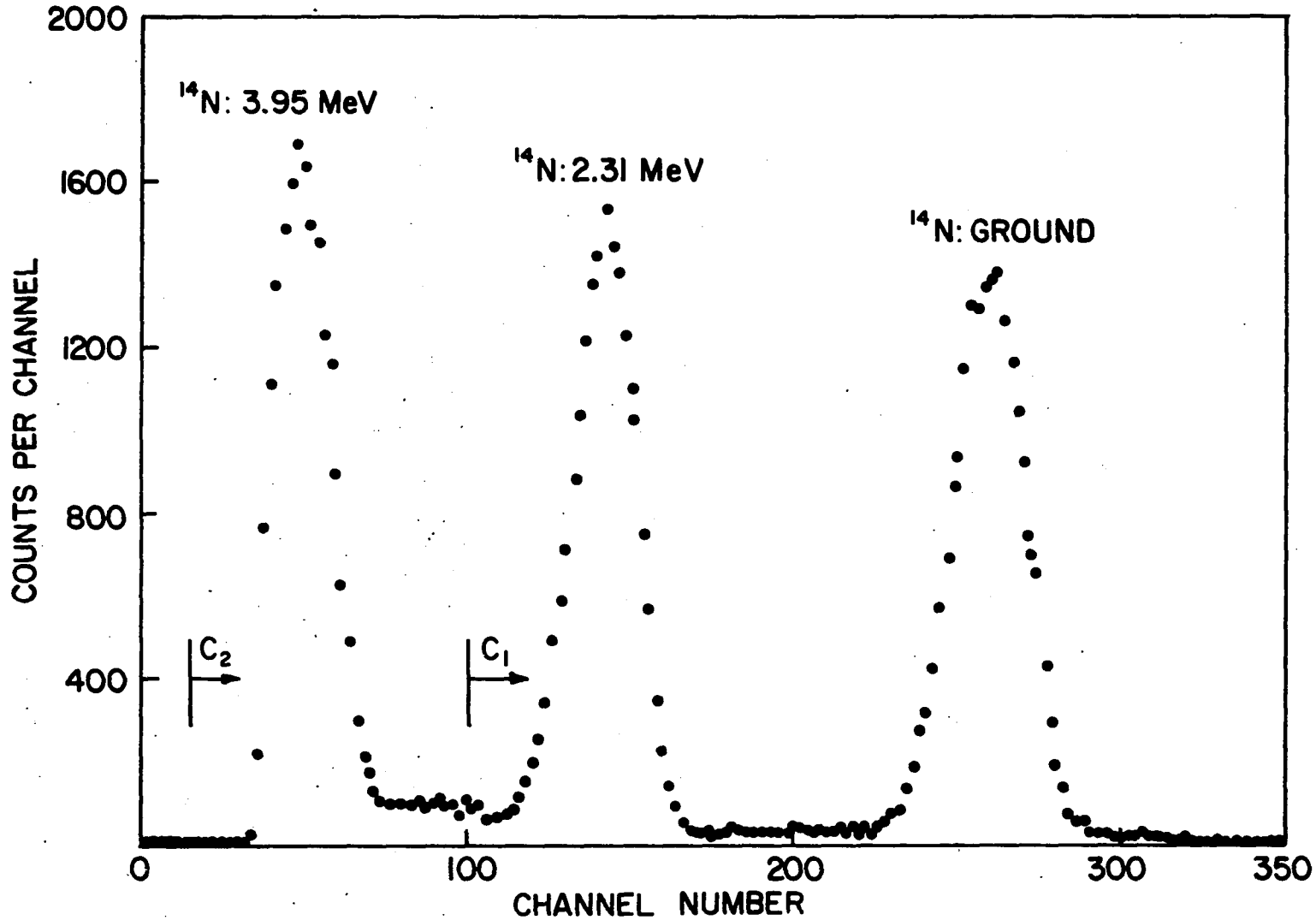
2000
1600
1200
800
400
COUNTS PER CHANNEL
^{14}N: 3.95 MeV
^{14}N: 2.31 MeV
^{14}N: GROUND
C2
C1
0
100
200
300
350
CHANNEL NUMBER

level discriminator on the amplifier for this detector was used to select the appropriate groups. The criterion used in the measurement of the mean life of the 2.31-MeV state is shown in the figure as C_1 and the criterion used in the measurements on the 3.95-MeV state is shown as C_2. In both cases no cascading effects were present and the number of chance coincidences caused by the inclusion of the proton groups associated with the formation of lower states was not sufficient to be troublesome.

The proton group from the formation of the 5.10-MeV state could not be separated from the elastically scattered ^{3}He ions, so that the coincidence technique could not be employed. However, the Q-value for the reaction producing this state is slightly negative. This means that the velocity of the recoiling ^{14}N will always be in the forward direction. The smallest value of the velocity occurs when the proton also proceeds in the direction of the beam. It is still possible to measure a shift, even for the smallest recoil velocity, if the average final velocity is not much less than the initial velocity. However, the range of mean lives that can be measured in this way is greatly reduced.

In all the experiments performed the γ rays were detected by a 3" x 3" NaI(Tl) crystal and photomultiplier. The front face of the crystal was placed 4" from the center of the target and its axis was in the plane defined by the

beam axis and the particle counter. A diagram of the experimental arrangement is shown in Figure 7. Two positions of the γ-ray detector are shown; in one position the γ-rays emitted along the direction of motion of the recoil nucleus are detected (solid lines) and in the other position the γ-rays emitted at 180° to this direction are detected (dashed lines). The diagram is schematic since the actual values of the angle between the recoil direction and the beam depend on the energy of the incident ^{3}He ion, the Q-value of the reaction and the location of the particle detector. In the actual experiment it was not always convenient to observe the γ rays at 0° and 180° to the recoil direction. Also the finite size at the NaI crystal implies that the angle of observation is not clearly defined but rather some average must be taken. Both of these effects can be accounted for in one equation

$$\cos\theta_1 - \cos\theta_2 \rightarrow \overline{\Delta\cos\theta}$$

$$= \frac{\sin\beta_1 - \sin\beta_1'}{\beta_1' - \beta_1} - \frac{\sin\beta_2 - \sin\beta_2'}{\beta_2' - \beta_2} . \qquad (18)$$

Here θ_1 and θ_2 are the average directions of observation referred to in the expression for the Doppler shift, equation (2). The angles β_i' and β_i are the values of the angle θ evaluated at the two edges of the front face of the NaI crystal when the axis of the crystal is at $\theta = \theta_i$. This

Fig. 7. The Experimental Arrangement. The angle, θ, defines the direction of the recoiling nucleus and therefore the position of the backward-looking γ-ray detection system. The dashed portion indicates the direction of the forward-looking γ-ray detection system.

EXPERIMENTAL ARRANGEMENT

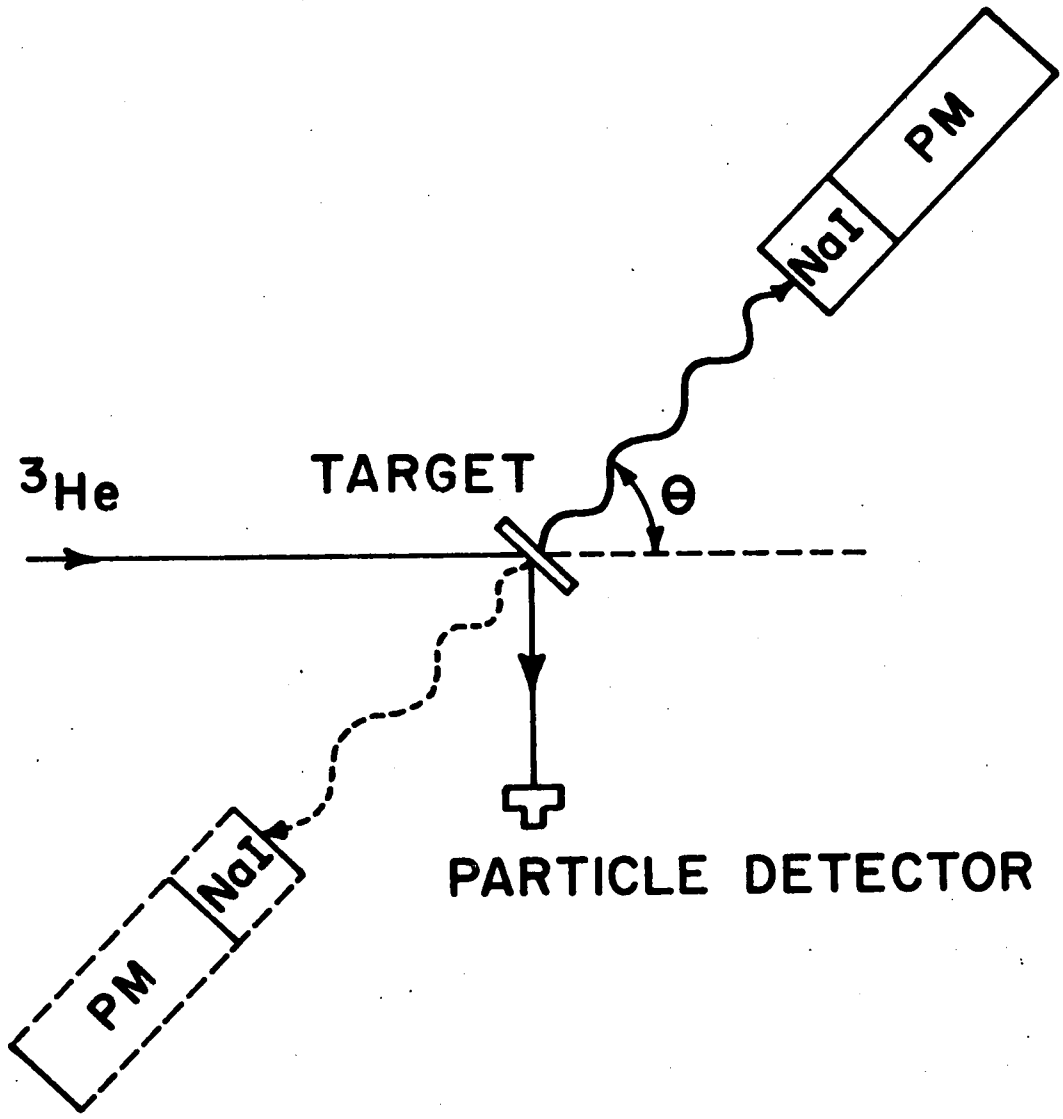

equation was derived by averaging cos θ over the front face of the crystal at the two positions referred to by the subscripts.

The pulses from the γ-ray detector were sorted and stored in a multichannel analyzer. The coincidence circuit was that incorporated in the analyzer and had a resolving time of 2 μsec. The data from the analyzer were plotted in order to locate the peaks graphically. In some cases background had to be subtracted in the manner described in section III A. Also the contributions from chance coincidences were subtracted from the peaks. The contributions were estimated from the measured chance coincidence rate using the singles (non-coincident) spectra to determine their shapes. The chance coincident peak was subtracted at the point of zero energy shift. In all cases where this correction was thought to be necessary it was made and in no case did the correction change the location of the peak beyond the error in locating it. The locations of the peaks were measured on all the data and the shift was determined from the differences in the average location of the peaks observed in the forward direction and of the peaks observed in the backward direction.

Since stopping-power data for either boron or nitrogen ions moving in copper and magnesium are not available, conversions were made from data for these ions in

nickel and aluminum which is displayed in a compilation by Northcliffe.[11] The stopping powers in this compilation have an estimated uncertainty of approximately 10%. The conversions were made using the theoretical formula developed by Lindhard and Scharff[12] for the electronic stopping power per atom which is

$$-\frac{d\epsilon}{dx} = \xi_e \frac{8\pi e^2}{a_o} \frac{Z_1 Z_2}{(Z_1^{2/3} + Z_2^{2/3})^{3/2}} \frac{v}{v_o}, \qquad (19)$$

where ξ_e is not a rapidly varying function of the properties of the stopping material. Z_1 and Z_2 are the charges of the moving ion and the stopping material. The constant, a_o, is the Bohr radius of the electron and e is its charge. v/v_o is the ratio of the velocity of the moving ion to $e^2/\hbar$. The formula agrees to within 15% of experimental values[3] of the stopping power for the region $0.35 \times 10^{-2} < v/c < 1.5 \times 10^{-2}$, where c is the velocity of light in a vacuum. However, when converting from one stopping material to another the dependence on velocity cancels; so it was assumed that this formula is a good approximation up to $v/c = 2.7 \times 10^{-2}$, corresponding to the highest initial velocity occurring in these experiments. The conversion was made by means of a multiplication factor as shown below

$$\left.\frac{dE}{dx}\right|_a = \left(\frac{A_b}{A_a}\right)\left(\frac{Z_a}{Z_b}\right)\left(\frac{Z_b^{2/3} + Z_\alpha^{2/3}}{Z_a^{2/3} + Z_\alpha^{2/3}}\right)^{3/2} \left.\frac{dE}{dx}\right|_b \qquad (20)$$

where A_i and Z_i are the atomic mass number and charge of the i^{th} stopping material and Z_α is the charge of the moving ion. The corrections applied to the data for nickel and aluminum to obtain stopping powers for copper and magnesium were themselves small (about 5%), and the errors introduced into the uncertainty in stopping power by these corrections were negligible compared to the experimental errors in the stopping-power data.

The stopping-power curves obtained were used to determine the parameters α, β and v' defined in section II A. The values of α, β and v' are subject to the restriction that because the stopping power is a continuous function of speed, the two approximations employed must be equal at the speed where they meet. This restriction implies that a choice of value for two of the three quantities α, β and v' fixes the value of the third. The procedure for determining the constants was to choose first a value of β which best approximated the stopping power for low speeds by a straight line passing through the origin as indiciated in Figure 1. Then a value of α was chosen such that the time required to reach the velocity, v', where the two approximations meet, is the same whether calculated from the approximation or from the data directly. The latter calculation can be made by integrating equation (4) to obtain a general expression for time, t, at velocity, v,

$$t = \int_{v_0}^{v} m\left(\frac{dE}{dx}\right)^{-1} dv. \qquad (21)$$

The integration can be performed graphically by plotting the integrand versus velocity and determining the area under that curve between the end points v and v_0.

In the determination of the mean life the finite thickness of the target must be accounted for since the target has a stopping power different from the backing materials. The correction for target thickness is made by determining the difference in time spent in the target and the time spent in an equivalent amount of backing material and adding this difference to the mean life determined from equation (10). The procedure is illustrated in Figure 8 where the integrand in equation (21) is plotted versus velocity. The lower curve corresponds to the backing material and the upper curve corresponds to the target material. The correction for the difference in stopping power is indicated by the shaded area which is defined by the two stopping powers and the velocities at which the ion enters and leaves the target material. The correction is about 0.3×10^{-14} sec for the cases described here and was applied only when the mean life was short enough for the correction to be significant.

The errors in the measurement of the mean lives arose from two independent sources, the uncertainty in the

Fig. 8. $M(dE/dx)^{-1}$ vs. Velocity. v_o is the initial velocity of the excited ^{14}N nucleus, v' is the velocity at which the ^{14}N leaves the target and enters the backing. The shaded area is proportional to the time added to correct for target thickness.

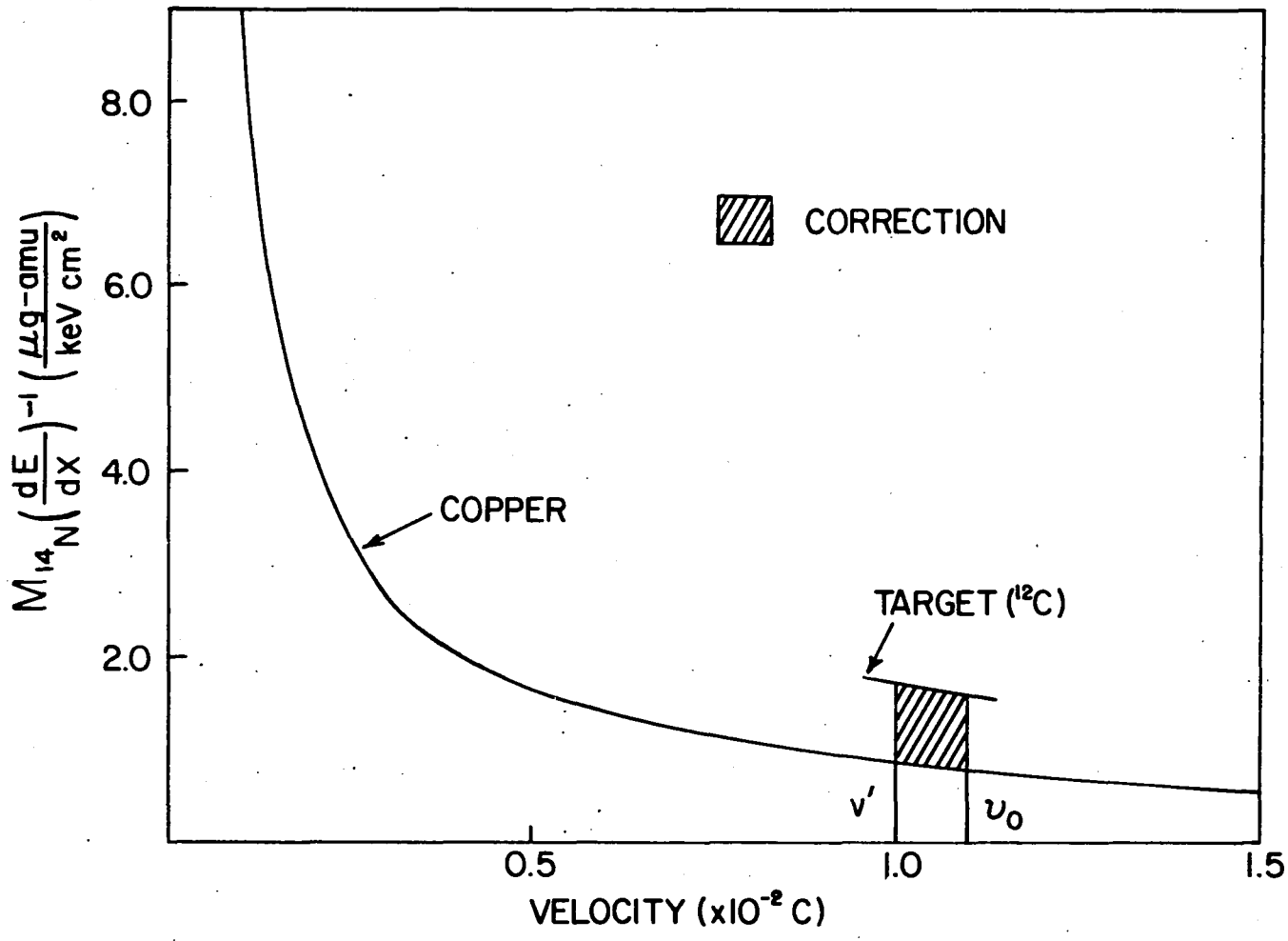
8.0
6.0
4.0
2.0
$M_{14_N}\left(\frac{dE}{dX}\right)^{-1}\left(\frac{\mu g\text{-amu}}{keV\ cm^2}\right)$
CORRECTION
COPPER
TARGET (^{12}C)
v'
v_0
0.5
1.0
1.5
VELOCITY ($\times 10^{-2}$ C)

stopping power. Each shift was calculated from about five measurements in each direction by averaging the shifts. The error was computed by taking the square root of the sum of squared deviations from the mean divided by n(n-1) where n is the number of measurements. Having thus compiled the error in the shift, the error in the determination of the average velocity is simply obtained from the rules of error propagation.[13] The error in the mean life is determined from the error in the average velocity by finding those values of τ in equation (10) which give the extreme values of the average velocity within its error.

The error due to the 10% uncertainty in the stopping power data is transmitted to the mean life through the parameters α, β and v'. In equations (5) and (7), where α and β are defined, it is seen that a 10% error in stopping power results in a 10% error in these two quantities. If in the expression for the average velocity (equation (3)) the integration is performed assuming the stopping power is constant for all velocities or assuming it is proportional to velocity for all velocities, the two results indicate that a 10% error in either α or β leads to a 10% error in the mean life. The experimental cases include both assumptions about stopping power. However, since the error is propagated to the same extent in both approximations, the percent error in the mean life due to uncertainties in the

stopping power will be the percent error in the stopping power, namely 10 percent. These two sources of error in the mean life contribute independently so that the total error is

$$\Delta\tau = \left[(0.1\tau)^2 + (\Delta\tau_{\overline{v}})^2 \right]^{\frac{1}{2}} , \qquad (22)$$

where $\Delta\tau_{\overline{v}}$ is the error due to uncertainty resulting from the shift measurement.

E. Angular Correlation

This section describes the measurement of the ratio of E2 and M1 multipole radiations in the 1.43-MeV transition from the 2.15-MeV state to the 0.72-MeV state in ^{10}B. The technique, described in section II B, requires the measurement of the angular distribution of the mixed γ radiation and the angular distribution of a pure multipole radiation from the same state. The pure multipole radiation used was that emitted in the 0.41-MeV transition from the 2.15-MeV state to the 1.74-MeV state. These two γ rays were observed in coincidence with the α particles observed along the beam direction from the formation of the 2.15-MeV state. The reaction used for this experiment was $^{11}B(^{3}He,\alpha)^{10}B$. A beam of ^{3}He ions at an energy of 2.0 MeV was used. The energy of the ^{3}He ions affects the experiment only in the number of 2.15-MeV states formed. As is seen from the excitation

functions, the higher the energy the greater the populations of this state.

The target was prepared by evaporating a relatively thick (about 150 $\mu g/cm^2$) film of enriched ^{11}B onto a piece of aluminum foil which was 6 mg/cm^2 thick. This thickness was chosen so that the 2.0-MeV ^3He ions are completely stopped in the aluminum yet the α particles from the formation of the 2.15-MeV state pass through the foil. The reason for this is that these α particles must be observed on the beam axis, but the α-particle detector would be destroyed if the beam were allowed to strike it directly.

A silicon surface barrier detector was used to detect the α particles. Its sensitive area was 25 mm^2 and it was placed 3.0 cm from the target along the beam axis. The detector pulses were amplified and discriminated with a single channel analyzer. The pulse height spectrum observed in this detector is shown in Figure 9. The peaks are labeled with the states whose formation is associated with the α particles producing the peak. The single channel analyzer opened the coincidence gate only when pulses with heights lying in the region designated GATE were observed. The α particles from the formation of the 2.15-MeV state were not resolved from those from the formation of the 1.74-MeV state. However, the angular distribution shows that the yield of the latter is a minimum at 0° while that of the

Fig. 9. Pulse-Height Spectrum of α Particles at 0° to the Beam. The reaction $^{11}B(^{3}He,\alpha)^{10}B$ was used with $E_{^{3}He} = 2.0$ MeV. The region, GATE, indicates the criterion for coincidence pulses in the angular correlation experiment.

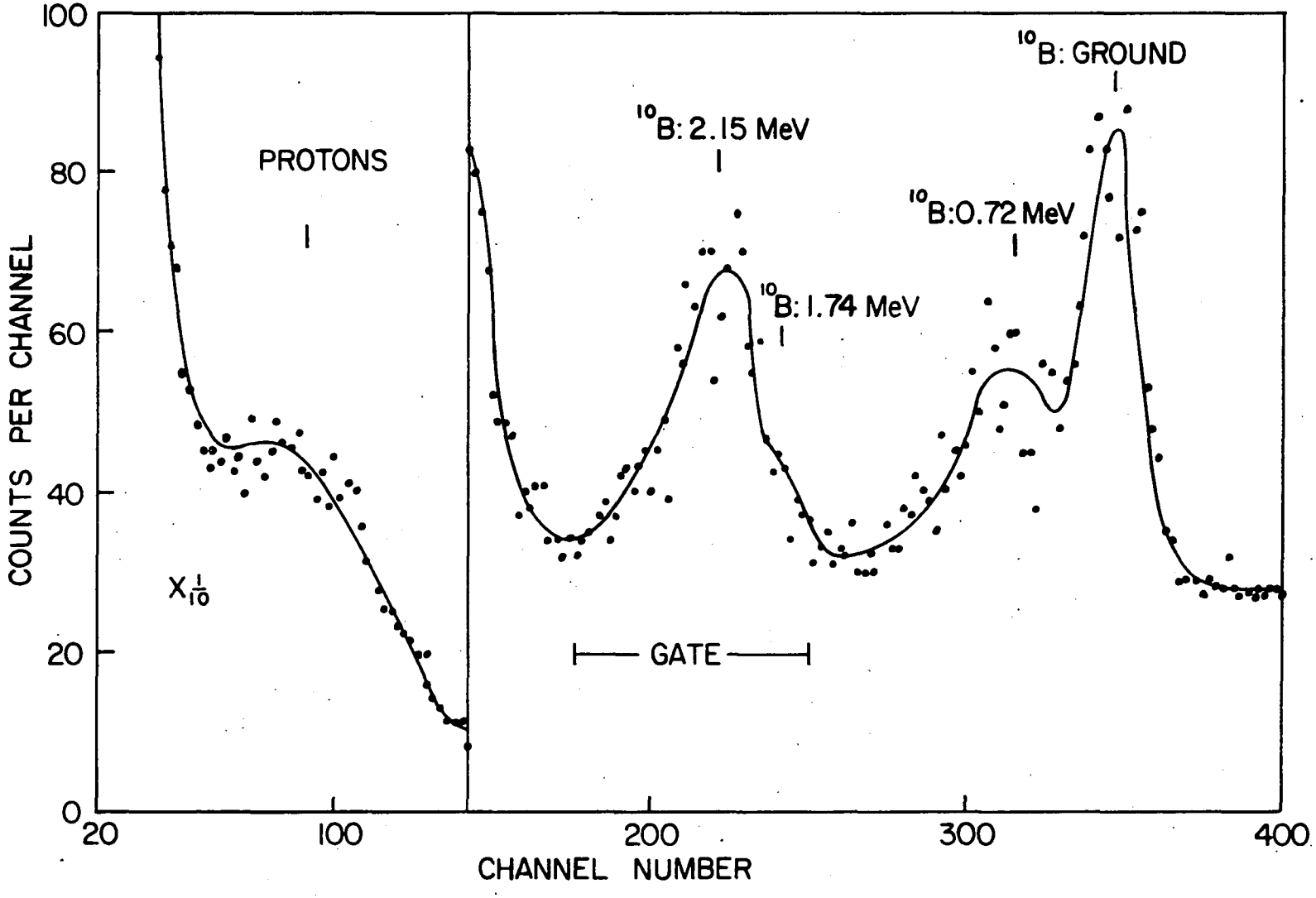
100
80
60
40
20
0
COUNTS PER CHANNEL
PROTONS
X 1/10
10B: 2.15 MeV
10B: 1.74 MeV
10B:0.72 MeV
10B: GROUND
GATE
20
100
200
300
400
CHANNEL NUMBER

former is a maximum at that angle. The effect of including both peaks in the coincidence criterion is to increase the chance coincidence rate by a negligible amount. In addition to opening the coincidence gate, the pulses from the single channel analyzer were also counted on a scaler. This provided a current monitor with which to normalize the γ-ray angular distribution.

The γ rays were detected in the NaI(Tℓ) crystal used in the other experiments, the front face of which was located 4" from the center of the target. The unnormalized angular distribution of γ rays from the 2.15-MeV state for which $J^{\pi} = 1^{+}$ is known[6] to have the form

$$W(\theta) = I_{\gamma}\left[1 + A_2(J_i,J_f)P_2(\cos\theta)\right], \qquad (23)$$

where I_{γ} is a constant depending on the exposure time and the beam current. The coefficient, $A_2(J_iJ_f)$, is the number that is needed to determine the mixing ratio and depends on the angular momenta of the initial and final states as well as the mixing ratio. For the present experiment the coefficient, $A_2(10)$, is associated with the distribution of the 0.41-MeV γ ray and $A_2(11)$ is associated with the 1.43-MeV γ ray. There are only two unknowns in equation (23), I_{γ} and $A_2(J_i,J_f)$; therefore, measurements of the intensity of the appropriate γ rays at two different angles completely determine the unknowns. However, to help eliminate any

systematic errors two separate measurements were made, each involving many runs. One was made at 0°, 125° and 55°, the other at 125° and 90°. The results were combined statistically.

The calculation used to determine f(x), and therefore the mixing ratio, are straight forward. For the case where W(0°) and W(55°) or W(125°) were measured, as can be seen from equation (23), the following equation gives A_2

$$A_2 = \frac{W(0°) - W(55°)}{W(55°)} . \qquad (24)$$

It should be noted that 55° and 125° are symmetric about 90°; therefore, the γ-ray yields are equal at 55° and 125°. Similarly, if W(90°) and W(55°) or W(125°) are measured then A_2 is given by

$$A_2 = -2\left[\frac{W(90°) - W(55°)}{W(55°)}\right] . \qquad (25)$$

Combining equations (12), (13) and (23) yields the result for f(x)

$$f(x) = -2\left[\frac{A_2(11)}{A_2(10)}\right] . \qquad (26)$$

The mixing ratio, x, is then determined from f(x) with the aid of equation (14).

The sources of error in this experiment are mainly statistical, that is they arise from the fact that $W(\theta)$ is the number of counts observed and thus has a statistical error given by $[W(\theta)]^{\frac{1}{2}}$. The fact that background occurred under the γ-ray peaks and had to be subtracted also contributed error. These two errors were treated together by measuring $W(\theta)$ several times and defining the error as the square root of the sum of squared deviations from the mean divided by $n(n-1)$, where n is the number of runs. The rules for the propagation of errors[13] were then strictly followed to obtain the error in the measurement of the mixing ratio. A possible source of systematic errors was that the physical apparatus might shield the detector from the γ rays to varying degrees depending on the angle. This possibility was checked by placing a radioactive source at the target position and observing the count-rate at the four angles used. Data were obtained with γ rays of energies 0.42-, 5.11-, 1.27-, 1.17- and 1.33-MeV. The appropriate corrections were applied to the distributions. Also, the target was rotated so as to minimize any attenuation by its support.

IV. RESULTS

A. Angular Distribution

The angular distributions of the α-particle yield about the beam direction from the reaction $^{11}B(^{3}He,\alpha)^{10}B$ were measured in the manner described in section III A. The groups resulting from the formation of the four lowest states in ^{10}B were observed for three ^{3}He energies, 1.0, 1.8 and 2.15 MeV. Two independent measurements of these angular distributions were made. Each point was obtained for a fixed number of monitor counts chosen so that the number of counts under the peaks to be measured was about 1000. In this manner, the statistical errors were kept somewhat uniform at 3 percent. Each point was taken in about ten minutes with a beam current of about 2.0 μa. A typical spectrum obtained is shown in Figure 3. The α-particle detector was placed at 90° in this case. The peaks are labeled by the state with whose formation the peak is associated. The peaks from reactions with ^{16}O and ^{10}B are the result of contamination of the target by these isotopes.

The angular distribution measured at ^{3}He energies of 1.0, 1.8, 2.15 MeV are displayed in Figures 10, 11 and 12, respectively. The distribution of α particles produced in the formation of the four lowest excited states of ^{10}B

Fig. 10. Angular Distributions for $E_{^3He} = 1.0$ MeV. α particles leading to the four lowest states in ^{10}B were formed by the reaction $^{11}B(^3He,\alpha)^{10}B$. The ^3He nuclei had an energy of 1.0 MeV. The curves are labeled with the state to which the α particles lead. The relative uncertainty is 10%. The absolute uncertainty is about a factor of two.

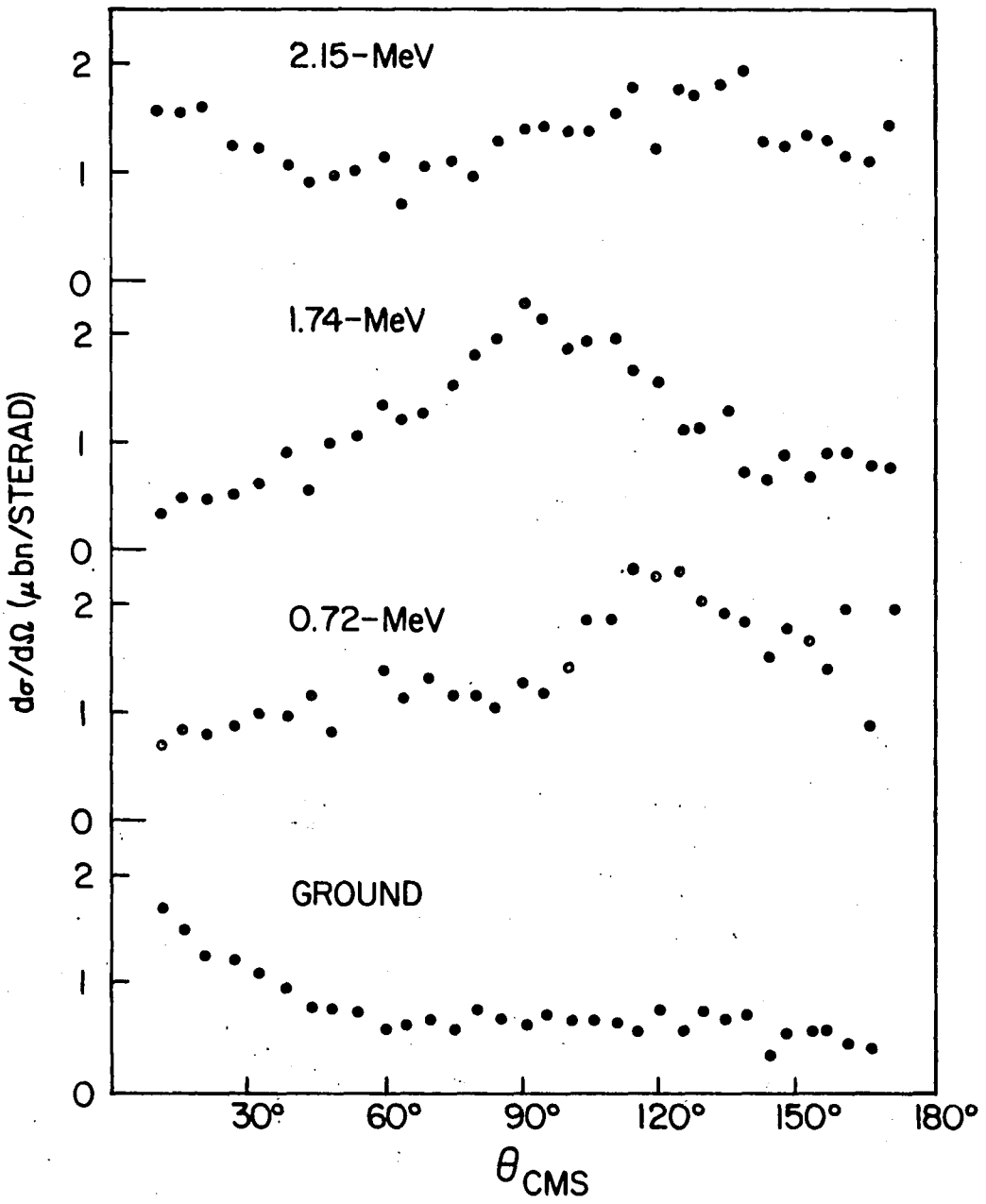
2.15-MeV
1.74-MeV
0.72-MeV
GROUND
dσ/dΩ (μbn/STERAD)
θCMS
30°
60°
90°
120°
150°
180°
0
1
2

Fig. 11. Angular Distributions for $E_{^3He} = 1.8$ MeV. α particles leading to the four lowest states in ^{10}B were formed by the reaction $^{11}B(^3He,\alpha)^{10}B$. The ^3He nuclei had an energy of 1.8 MeV. The curves are labeled with the state to which the α particles lead. The relative uncertainty is 5%. The absolute uncertainty is about a factor of two.

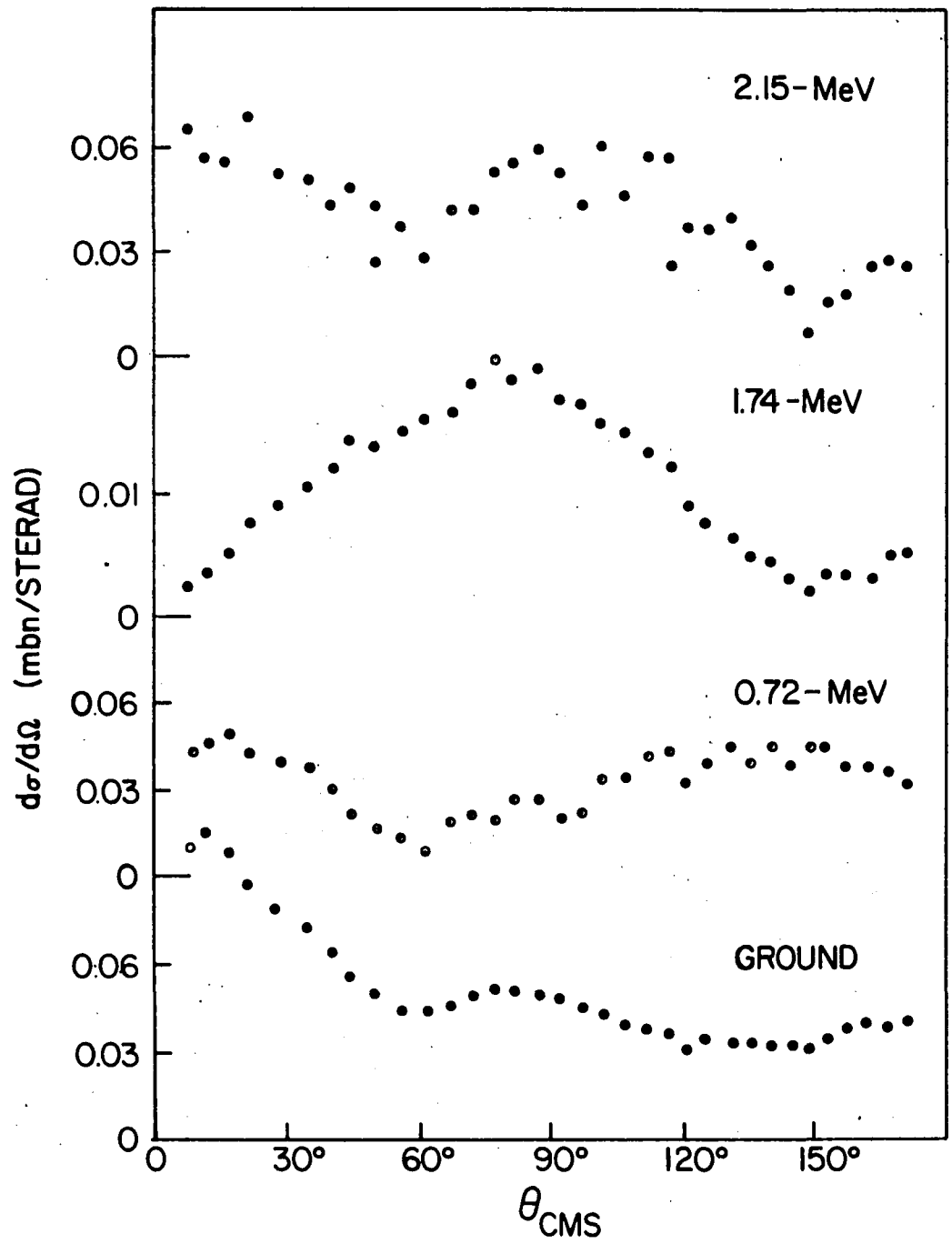
2.15-MeV
1.74-MeV
0.72-MeV
GROUND
0.06
0.03
0
0.01
0
0.06
0.03
0
0.06
0.03
0
0
30°
60°
90°
120°
150°
θCMS
dσ/dΩ (mbn/STERAD)

Fig. 12. Angular Distributions for $E_{^3He} = 2.15$ MeV. α particles leading to the four lowest states in ^{10}B were formed by the reaction $^{11}B(^3He,\alpha)^{10}B$. The ^3He nuclei had an energy of 2.15 MeV. The curves are labeled with the state to which the α-particles lead. The relative uncertainty is 5%. The absolute uncertainty is about a factor of two.

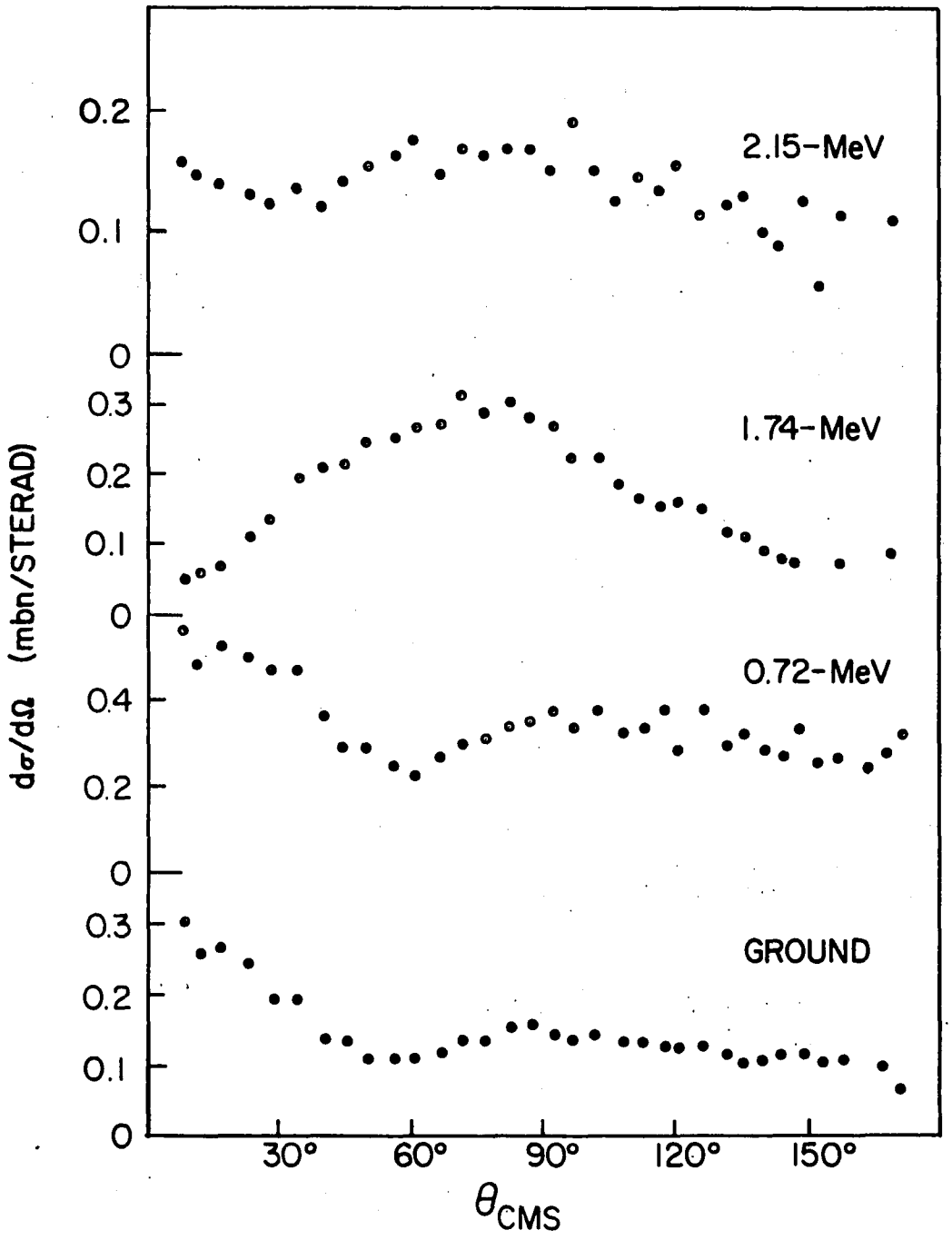
2.15-MeV
1.74-MeV
0.72-MeV
GROUND
0.2
0.1
0
0.3
0.2
0.1
0
0.4
0.2
0
0.3
0.2
0.1
0
30°
60°
90°
120°
150°
θCMS
dσ/dΩ (mbn/STERAD)

are plotted in the figures and labeled according to the appropriate state formed. The ordinate is the differential cross section in mbn per sterad. The absolute value of the differential cross section was obtained from the thickness of the foil determined by weighing and the measured beam current.

The relative statistical error is 3%. Other errors occur in the backward directions because the four body break-up of ^{13}N, described in section III A, contributes a large background at lower energies. Another source of error is the fact that peaks from α particles produced in other reactions, (e.g. $^{16}O(^{3}He,\alpha)^{15}O$) lie close to, or beneath, the peaks of interest. Both these effects were corrected for by estimating the background produced and subtracting that from the peaks. The errors so introduced are reflected in the scatter of points.

The error in the absolute value of the differential cross section is estimated to be about a factor of two. There are two sources which give rise to this large error both of which lead to a small value for the cross section. One source results from the uncertainty in foil thickness produced by the presence of an unknown amount of tantalum evaporated with the boron. Since tantalum is a heavy element, a relatively small number of atoms can cause a large error in the determination, by weighing, of the amount of boron present. The other source of error was the uncertainty in

the beam current. The value used was that current which was observed when the beam was on target. Since the beam does drift occasionally the average current could be somewhat lower than this value. No corrections were made for these errors other than to roughly estimate their maximum effect by comparing these data to that obtained at higher energies for this reaction[14] and by comparing the results of various methods (including weighing) for determining the thickness of ^{10}B foils prepared by evaporation from tantalum.[15] The maximum effect was used to set the error. This large error does not detract from the analysis which attempts to fit only the shape of the distribution.

B. Excitation Function

The results of the measurements of the excitation function for the formation of the five lowest states in ^{10}B by the reaction $^{11}B(^{3}He,\alpha)^{10}B$ are shown in Figure 13. The ordinate is the differential cross section in mbn/sterad obtained at 90° to the beam. The abscissa is the energy of the incident ^{3}He nuclei in MeV. Each excitation function is labeled by the state formed in the reaction. The points were taken for a fixed amount of charge recorded by the current integrator. The absolute error of the differential cross section is about a factor of two and was estimated in the same manner as was described for the angular distributor in section IV A. The relative error varies with energy

Fig. 13. Excitation Functions. Excitation functions for the formation of the five lowest states in ^{10}B through the reaction $^{11}B(^{3}He,\alpha)^{10}B$ are shown. The points indicate the α particle yield at 90° to the beam direction. Their relative uncertainty is 5% and the absolute uncertainty is about a factor of two. The dashed line is derived from barrier penetration theory.

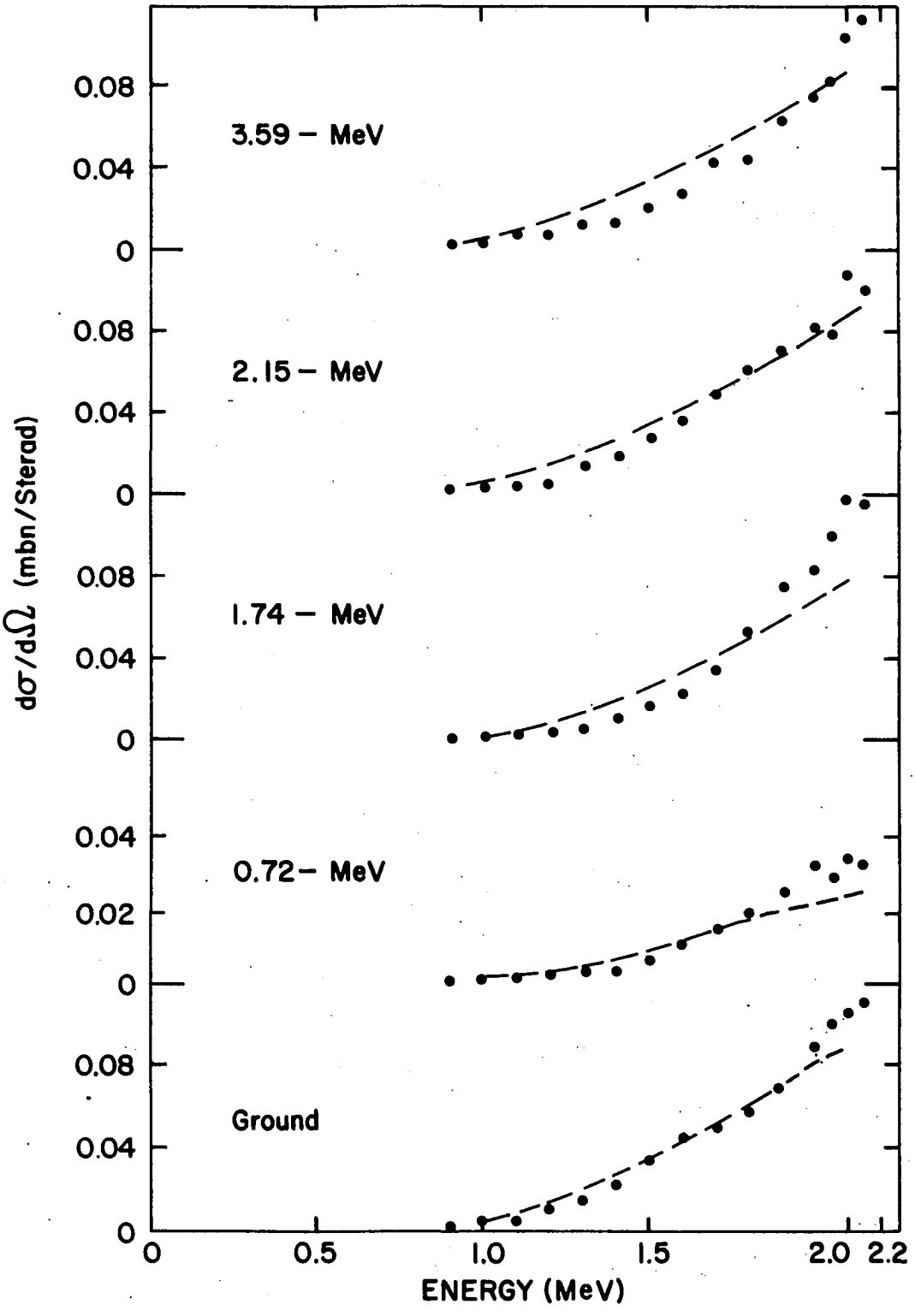
3.59 – MeV
2.15 – MeV
1.74 – MeV
0.72– MeV
Ground
dσ/dΩ (mbn/Sterad)
ENERGY (MeV)
0.08
0.04
0
0.02
0.5
1.0
1.5
2.0
2.2

since it depends on the yield which was low at low energies. This error was computed statistically and is about 20% at $E_{^3He}$ = 1.0 MeV and about 4% at $E_{^3He}$ = 2.15 MeV.

The shape of the excitation function is indicative of the fact that the ^3He energies are less than the coulomb barrier which is at about 4 MeV. The excitation function is compared with a curve (dashed line in Figure 13) computed from an expression for potential barrier penetration developed by Blatt and Weisskopf.[16] The table of Charged Particle Penetrabilities by Schiffer[17] was used in the calculation. The orbital angular momentum quantum number in the incident channel was assumed to be zero in all but the case of the formation of the 1.74-MeV state. In this case this quantum number was taken to be one in order to conserve angular momentum. That this is required is the result of assuming that an $s_{\frac{1}{2}}$ neutron is picked up in this case. This matter is discussed in more detail in section V A. The calculations appear to be in reasonable agreement with the experimental points.

C. Mean Lives of the Excited State of ^{10}B

1. 1.74-MeV State

The mean life of the 1.74-MeV state in ^{10}B was determined from the Doppler shift of the 1.02-MeV γ ray from the 1.74 → 0.72-MeV transition, the only one which occurs.

An example of the coincidence spectra obtained with the discriminator set at criterion C_1 (see Figure 4) is shown in Figure 14. The 0.511-MeV peak in the spectrum results from chance coincidences of annihilation radiation from the positron decay of ^{13}N produced by $^{11}B(^{3}He,n)^{13}N$ reactions. The 0.41-MeV γ rays came from the 2.15 → 1.74-MeV transition in ^{10}B and from neutron-induced reactions in the NaI(Tℓ) crystal. The other γ rays are from the other transitions in ^{10}B indicated in the figure. As mentioned above, when measuring the shift of the 1.02-MeV peak the fact that the 2.15-MeV state decays about one-third of the time through the 1.74-MeV state must be taken into account. The magnitude of this contribution was determined by estimating the population of the 2.15-MeV state relative to the 1.74-MeV state from the ratio of counts in the 1.02-MeV peak to those in the 1.43-MeV peak produced by transitions from the 2.15-MeV state to the 0.72-MeV state. This ratio combined with differences in counting efficiency and the known branching ratios of the 2.15-MeV state[18] showed that less than one-seventh of the 1.02-MeV peak resulted from cascades from the 2.15-MeV state. The effect of the contribution of these cascade γ rays was shown to be too small to be seen in these measurements.

The reason the 0.41-MeV peak was not used to estimate the magnitude of this correction is that much of that peak

Fig. 14. Pulse-Height γ-Ray Spectrum for Measurements on the 1.74-MeV State in ^{10}B. These γ rays are in coincidence with α particles satisfying the criterion C_1 of Fig. 3. This is typical of the spectra used to determine the mean life of the 1.74-MeV state in ^{10}B. The multichannel-analyzer sensitivity was set so as to count only channels above 60.

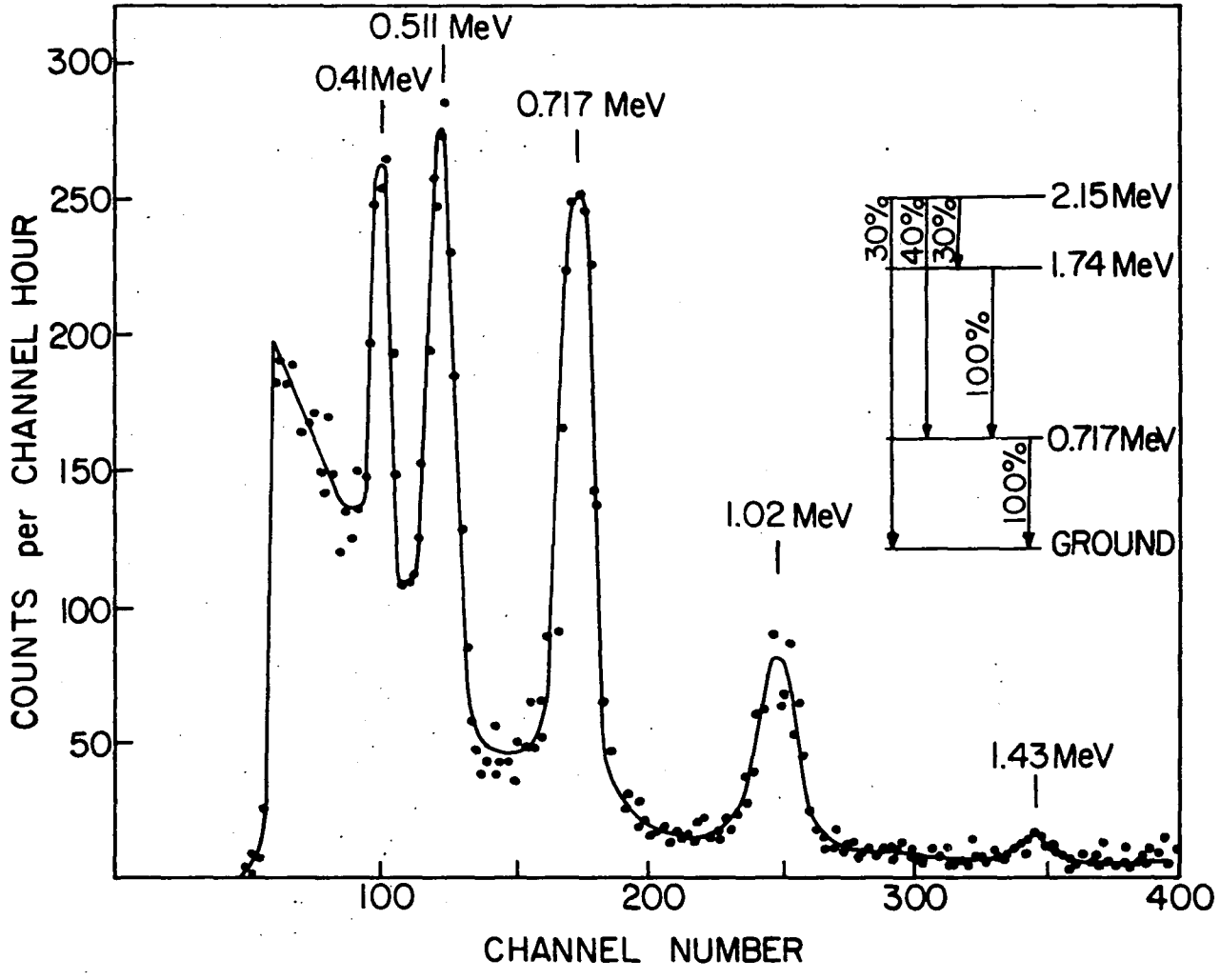
0.511 MeV
0.41MeV
0.717 MeV
1.02 MeV
1.43MeV
2.15MeV
1.74 MeV
0.717MeV
GROUND
30%
40%
30%
100%
100%
COUNTS per CHANNEL HOUR
CHANNEL NUMBER
300
250
200
150
100
50
100
200
300
400

resulted from chance-coincident γ rays from neutron-induced reactions in the NaI(Tℓ) crystal. The excitation of states around 0.4 MeV in the NaI(Tℓ) crystal was the result of inelastic scattering of neutrons produced in the reactions $^{11}B(^{3}He,n)^{13}N$. A separate measurement using a Pu-Be neutron source was made to determine the intensity of the γ rays from this process. Alpha particles from an ^{241}Am source were used to provide random pulses to the coincidence gate at a known rate and the chance-coincident γ rays produced by (n,n') reactions in the crystal were then counted. By this procedure, it was found that the γ rays from the neutrons inelastically scattered in the detector crystal were sufficient to account for about 50% of the 0.41-MeV peak in Figure 14.

After subtracting the background and making the correction for the unshifted 1.02-MeV γ rays in the cascade from the 2.15-MeV state, the shift from five runs in the forward and backward directions was determined to be 7.25 ± 0.5 channels in 246 channels. This shift was measured by referring the individual peaks to the unshifted peak from the 0.72-MeV γ ray. The error is the square root of the sum of squared deviations from the sample mean. This shift corresponds to a mean final velocity of $(4.62 \pm .33) \times 10^{8}$ cm/sec. The mean life of the 1.74-MeV state was determined through equation (10) to be $(1.90 \pm 0.30) \times 10^{-13}$ sec. The error was computed in the manner described in section III D. The

two sources of error contributed approximately equally to the total error.

2. 2.15-MeV State

The mean life of the 2.15-MeV state was determined from the Doppler shift of two of its three possibly decay modes; the 0.41-MeV γ ray from the 2.15 → 1.74-MeV transition, and the 1.43-MeV γ ray from the 2.15 → 0.72-MeV transition. For measurements on this level, a magnesium-backed target was used. An example of the coincidence spectra obtained with the α-particle discriminator set at C_2 (see Figure 4) is shown in Figure 15. For this spectrum the discriminator was set to pass all pulses produced by α particles to the 2.15-MeV state. As a result, the number of 0.41-MeV γ rays in true coincidence with α particles was much larger than the number of 0.41-MeV γ rays from chance coincidences. This is in contrast to the situation depicted in Figure 14. The 0.41-MeV γ-ray peak had good statistics and the proximity of the 0.511-MeV annihilation peak offered a good reference from which to measure the shift. However, since the Doppler shift is proportional to the γ-ray energy, in this case it was small and difficult to measure accurately. Four independent hour-long runs in each direction were made giving a Doppler shift of 0.55 ± 0.13 channels in 85 channels. The error is again the square root of the sum of squared deviations from the sample mean. This shift corresponds to a mean final velocity of $(10.5 \pm 2.4) \times 10^7$ cm/sec.

Fig. 15. Pulse-Height γ-Ray Spectrum for Measurements on the 2.15-MeV State in ^{10}B. These γ rays are in coincidence with α particles satisfying the criterion C_2 of Fig. 3. This is typical of the spectra used to determine the mean life of the 2.15-MeV state in ^{10}B. The multichannel-analyzer sensitivity was set so as to count only in channels above 60.

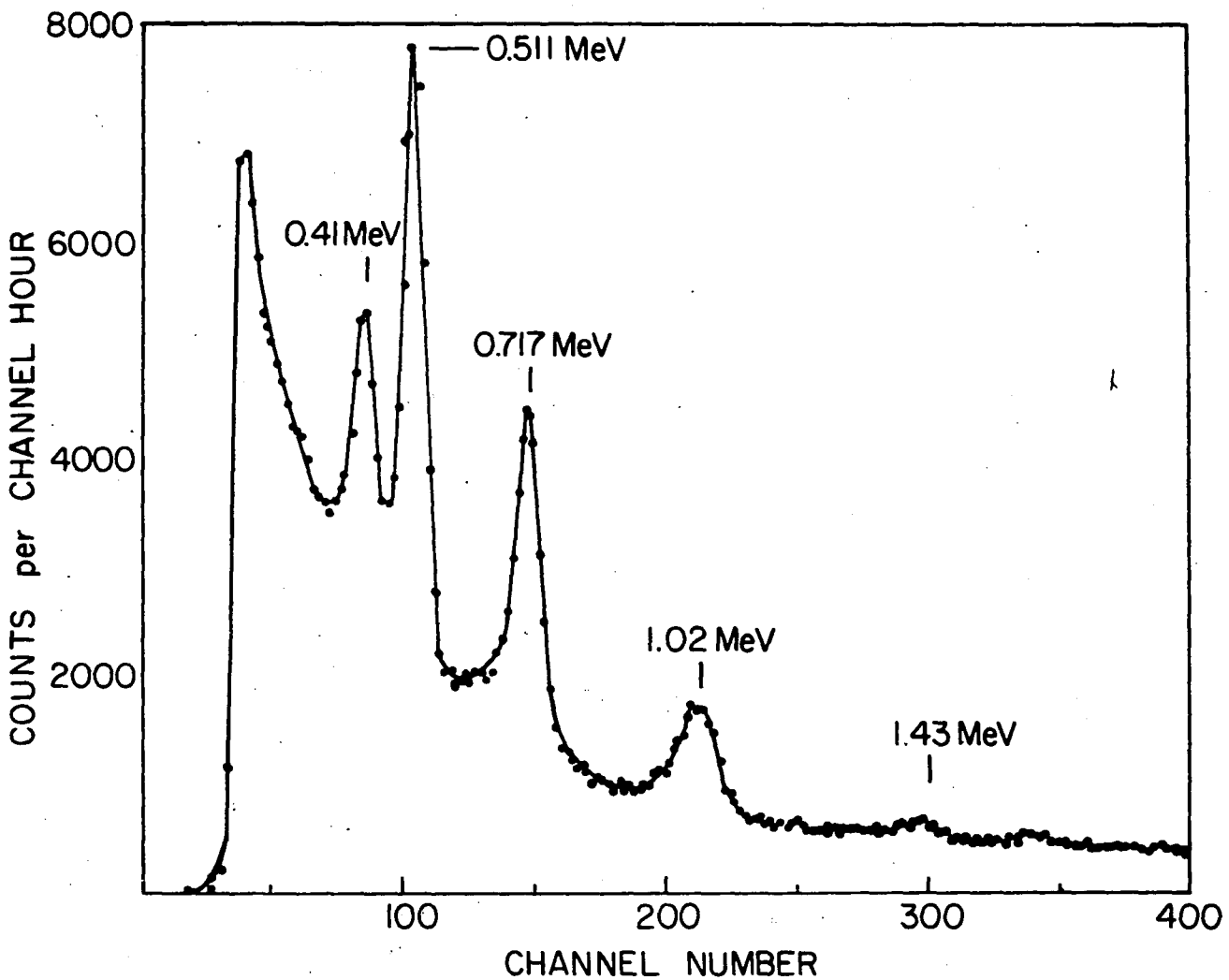
8000
6000
4000
2000
COUNTS per CHANNEL HOUR
0.511 MeV
0.41 MeV
0.717 MeV
1.02 MeV
1.43 MeV
100
200
300
400
CHANNEL NUMBER

Although the shift of the 1.43-MeV γ-ray peak was three times that of the 0.41-MeV γ-ray peak, the 1.43-MeV peak had poor statistical accuracy. The shift was measured from the same four runs described above and was 1.6 ± 0.8 channels in 300 channels, which gives a mean final velocity of (9.0 ± 4.5) x 10^7 cm/sec. Part of the inaccuracy of this shift measurement was due to the lack of a close reference peak. The peaks from the 0.71-MeV and 0.511-MeV γ rays were used as references. The value adopted for the mean final velocity was (10.2 ± 2.4) x 10^7 cm/sec. This velocity together with the stopping-power data gave 5^{+2}_{-1} x 10^{-12} sec for the mean life of the 2.15-MeV state. The mean life was sensitive to the error in the measurement of the mean final velocity, since this mean life is near the upper limit of times that can be measured by this method. This error and the 10% uncertainty in the stopping-power were combined in the manner described in section III D.

3. 3.58-MeV State

The Doppler shift of the 2.89-MeV γ ray from the transition between the 3.58- and 0.72-MeV states in ^{10}B was measured using a copper backing in order to obtain the mean life of the 3.58-MeV state. Although this state decays to other lower states the above transitions was the only one which could be clearly identified in the coincidence spectra. An example of the spectra obtained with the coincidence

circuit gated on the α particles from the formation of the 3.58-MeV state (see Figure 5) is shown in Figure 16. The peaks have been previously identified. The gain of the γ-ray detection system was stabilized electronically so that the peaks drifted less than $\frac{1}{4}$ channels throughout the experiment. A total of six runs were made at each of the two γ-ray detector positions. Although the peak is difficult to see it was consistently located in all the runs. However, since the peaks were weak, the two sets of three runs were added separately in the forward and backward cases. Thus two determinations of the shift were made from the data combined in this way and the results were consistent with the other determination. The 2.89-MeV γ-ray peak could be clearly seen in the combined spectrum. The reason that runs long enough to produce the equivalent of the combined spectrum were not made was that, because the ^{3}He beam current could not be maintained above 0.5 μa for extended periods and because the counting efficiency for γ rays with this energy is low, the runs made averaged about 3 hours in duration. The shift in the 2.89-MeV γ ray was 76 ± 20 keV. This corresponds to a mean final velocity of $(4.50 \pm 0.7) \times 10^{8}$ cm/sec which in turn gives the value $(1.75 \pm 0.70) \times 10^{-13}$ sec for the mean life of the 3.58-MeV state. The errors from the determination of the mean final velocity dominated the errors resulting from the stopping power uncertainty.

Fig. 16. Pulse-Height γ-Ray Spectrum for Measurements on the 3.58-MeV State in ^{10}B. These γ rays are in coincidence with α particles satisfying the GATE criterion of Fig. 4. This is typical of the spectra used to determine the mean life of the 3.58-MeV state in ^{10}B.

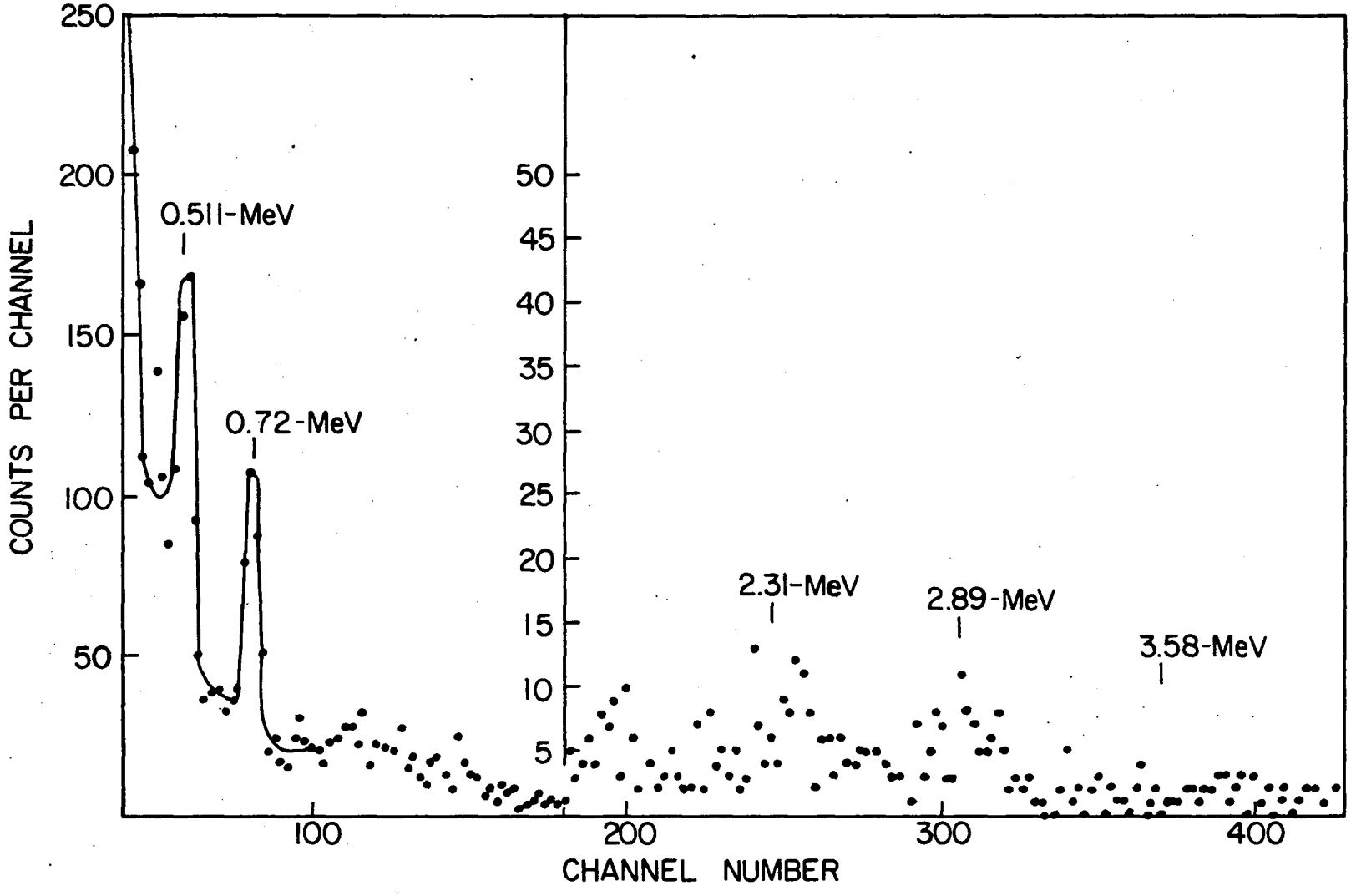
250
200
150
100
50
50
45
40
35
30
25
20
15
10
5
0.511-MeV
0.72-MeV
2.31-MeV
2.89-MeV
3.58-MeV
COUNTS PER CHANNEL
100
200
300
400
CHANNEL NUMBER

D. Mean Lives of Excited State in ^{14}N

1. 2.31-MeV State

The mean life of the 2.31-MeV state in ^{14}N was measured from the shift of the ground state transition. An energy level diagram for this nucleus[18] is shown in Figure 17 where the levels are labeled by their energy, spin, parity and isotopic spin. A copper backing was used and the shift was measured relative to a reference peak. In Figure 18 examples of spectra used to measure the mean lives of three excited states in ^{14}N are shown together. Only the part appropriate to the 2.31-MeV state, part (a), will be discussed here; the other parts will be discussed in the following sections. In Figure 18(a) the 2.31-MeV γ ray from the decay of that state is shown along with the 2.75-MeV reference peak. This spectrum was obtained in coincidence with protons satisfying the criterion C_1 (see Figure 6). The reference peak appears by chance coincidence and was produced by γ rays from the decay of a ^{24}Na radioactive source that was placed near the detector. The location of the Doppler-shifted peak was determined relative to this reference peak.

Measurements of the Doppler shift gave a value for the mean final velocity of the ^{14}N nuclei in this state of $(2.55 \pm 0.24) \times 10^8$ cm/sec, which corresponds to a mean life of $(8.3 \pm 3.0) \times 10^{-14}$ sec for the state. The error is a

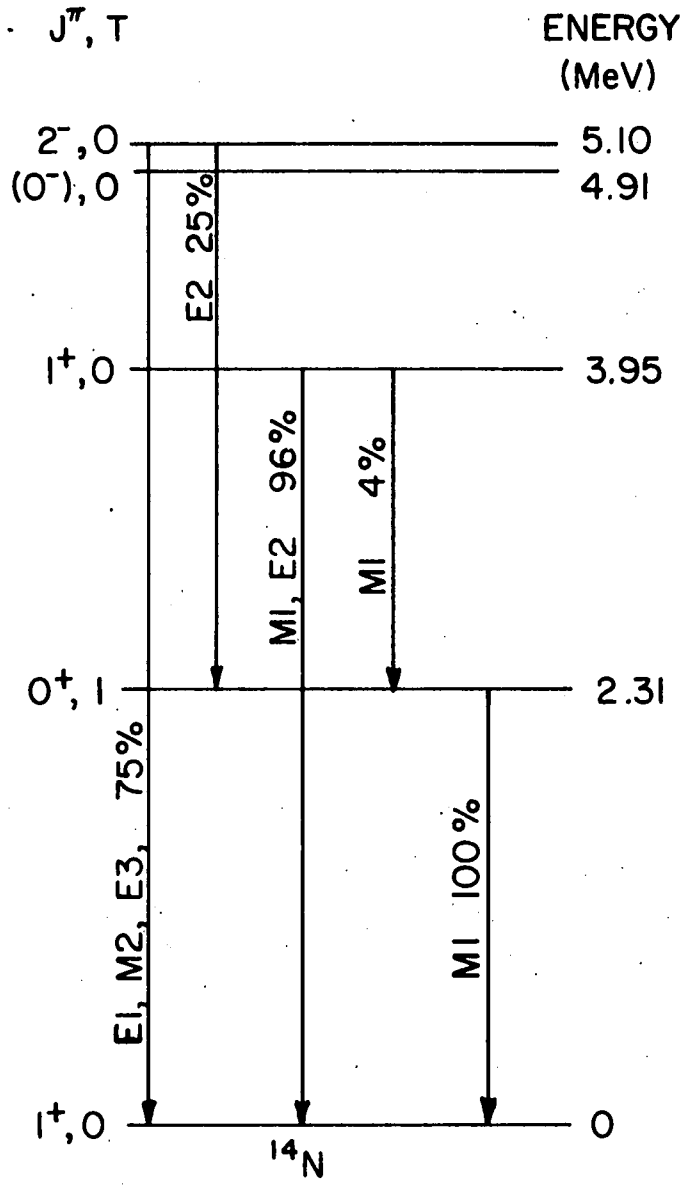

Fig. 17. Energy Level Diagram for ^{14}N.

Fig. 18. Pulse-Height γ-Ray Spectrum for Measurements on States in ^{14}N. These γ ray peaks are a) from the 2.31 MeV → g.s. transition in ^{14}N and from a ^{24}Na reference source, b) from the 3.95 → 2.31 MeV transition in ^{14}N and from a ^{24}Na reference source and c) from the 5.10 MeV → g.s. transition in ^{14}N and from a Pu-Be source.

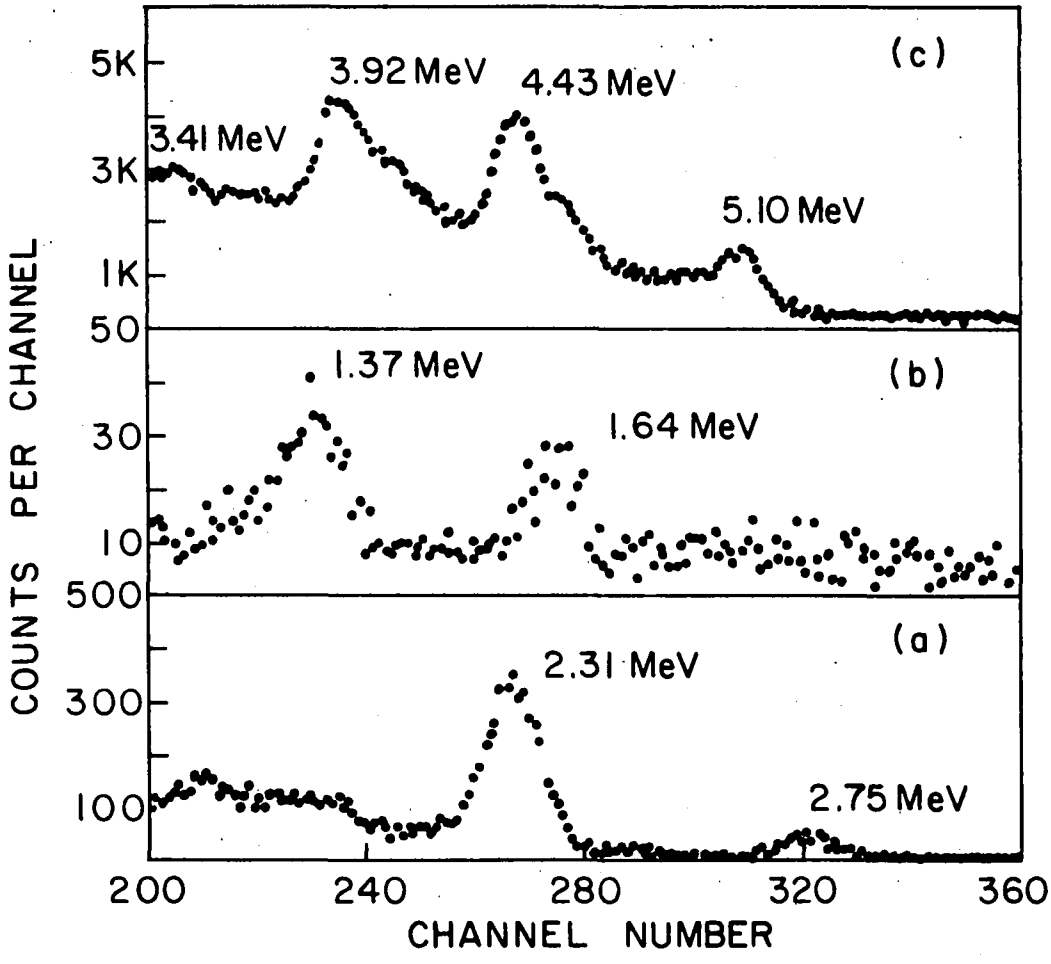
5K
3K
1K
50
30
10
500
300
100
3.92 MeV
4.43 MeV
3.41 MeV
5.10 MeV
(c)
1.37 MeV
1.64 MeV
(b)
2.31 MeV
2.75 MeV
(a)
COUNTS PER CHANNEL
200
240
280
320
360
CHANNEL NUMBER

combination of the uncertainty in the Doppler-shift measurement, determined from a statistical analysis of several measurements of that quantity and from uncertainties in the stopping powers used to compute the mean life. In this case the error in the velocity measurement was more important than the error in stopping power. This result agrees with previous values obtained by Swan et al.[19] ($(7.1 \pm 1.8) \times 10^{-14}$ sec) and by Booth et al.[20] ($(9.7 \pm 3.0) \times 10^{-14}$ sec) using resonance fluorescence techniques.

2. 3.95-MeV State

The 3.95-MeV state decays to both the ground state and the 2.31-MeV state (see Figure 17). The γ ray from the transition to the latter was used for the Doppler-shift measurement. In Figure 18(b) an example of the spectra obtained in coincidence with protons satisfying criterion C_2 (see Figure 6) is shown. Here the 1.64-MeV γ-ray peak from the decay of the 3.95-MeV state to the 2.31-MeV state appears along with the 1.37-MeV γ-ray reference peak. The location of the shifted peak was determined relative to this reference peak. The reference peak was produced by a ^{24}Na radioactive source and occurred in the spectrum by chance coincidences with the protons. The Doppler shift was determined to be 31.6 ± 2.1 keV from six hour-long runs made in each direction. This is the maximum possible shift allowed by the kinematics of the reaction so that from these measurements only an upper limit can be placed on the mean life of

the state. The value of this limit is chosen to be that mean life that would correspond to a mean final velocity which is less than the initial velocity by an amount corresponding to the error in the shift measurement, using, in the computation, the lowest values of stopping power consistent with their uncertainty. The limit defined in this way was $\tau \leq 2.5 \times 10^{-14}$ sec.

3. 5.10-MeV State

As was mentioned before, the protons from the formation of the 5.10-MeV state were not resolved so that the Doppler shift of decay γ radiation from this state must result from center of mass motion. An example of the non-coincident spectra used to determine the shift is shown in Figure 18(c). The 5.10-MeV γ-ray peak produced by the ground state transition is shown. This γ ray was used for the measurements on the 5.10-MeV state. Also appearing in the spectrum is the 4.43-MeV reference peak along with the peaks from the first and second escape of that γ ray. The reference γ rays were produced by a Pu-Be source. Six measurements on the 5.10-MeV γ rays in forward and backward directions yielded no detectable Doppler shift relative to the reference peak. Thus ^{14}N nuclei in the 5.10-MeV state are stopped on the average before emitting γ rays. Only a lower limit to the mean life can be obtained. Since coincidences were not used in this measurement, to obtain a

limit for the mean life, it was necessary to estimate the average initial velocity of the recoiling nuclei in this state. Since an accurate determination of such a velocity would require detailed knowledge of the differential cross section, a conservative estimate of that velocity was made. The smallest initial velocity in the above average occurs for the case where the proton proceeds in the forward direction, and this velocity was used as the initial velocity. A mean final velocity corresponding to the largest shift which would not be detected was determined. These two extreme values were then used to compute a mean life which was taken to be the lower limit. Thus the mean life of the 5.10-MeV state was computed to be $\tau > 2 \times 10^{-12}$ sec.

For convenience the results of the mean life measurements are summarized in Table II. In this table the state is identified in the first two columns. The next two columns list the initial and mean final velocities of the recoiling nuclei. The fifth column lists the measured mean lifes and the last column lists the total widths which are related to the mean lives by the relation Γ (ev) τ (sec) = 6.58×10^{-16}.

E. Mixing Ratio

The angular distributions of the two γ rays from the decay of the 2.15-MeV state were measured as described in section III E. These measurements were made at 90° and 125°

TABLE II

Summary of Measured Mean Lives

Nucleus	State (MeV)	$\frac{v_o}{c} \times 10^{-2}$	$\frac{v_f}{c} \times 10^{-2}$	Measured Mean Life (sec)	Total Widths ($\times 10^{-3}$ ev)
^{10}B	3.58	2.36	1.49 ± 0.23	$(1.75 \pm 0.70) \times 10^{-13}$	3.75 ± 1.3
^{10}B	2.15	2.69	0.35 ± 0.08	$5^{+2}_{-1} \times 10^{-12}$	$.13 \pm 0.035$
^{10}B	1.74	2.53	1.54 ± 0.11	$(1.90 \pm 0.30) \times 10^{-13}$	3.5 ± 0.6
^{14}N	5.10	0.41	< 0.05	$> 2 \times 10^{-12}$	< 0.33
^{14}N	3.95	1.07	1.06 ± 0.07	$< 2.5 \times 10^{-14}$	> 26
^{14}N	2.31	1.17	0.85 ± 0.15	$(8.3 \pm 3.0) \times 10^{-14}$	7.9 ± 3.0

in one experiment and at 0°, 55° and 125° in another. In both cases several runs were made for a fixed number of monitor counts, that is, for a fixed number of α particles from the formation of the 2.15-MeV state proceeding in the forward direction. This number corresponded to about 1.8×10^{-3} coulombs of beam charge. Examples of γ-ray spectra observed at 125° and 90° to the incident beam are displayed in Figure 19 a and b, respectively. The peaks are labeled by the energy of the γ ray producing them. Their origins are discussed with reference to Figure 14 in section IV D.

The coefficients, $A_2(10)$ and $A_2(11)$ were determined in the manner described in section III E and the function f(x) was found to be 1.35 ± 0.78 in the first experiment and 0.98 ± 0.50 in the second experiment. The reason the latter is more accurate is that the dependence of f(x) on A_2 at 0° is twice as strong as its dependence at 90° as can be seen from equations (23) and (25). The statistical average of these values is 1.05 ± 0.41. The mixing ratio was determined with equation (15) by picking the value of x which give the measured value of f(x). The ratio, x, of amplitudes of E2 and M1 multipole radiation in the 1.43-MeV transition from the 2.15-MeV state to the 0.72-MeV state in ^{10}B was determined to be $|x| < 0.07$. That is, within the accuracy of the experiment no quadrupole radiation was observed. This

Fig. 19. Pulse-Height γ-Ray Spectrum for Angular Correlation Measurements. These γ rays are in coincidence with α particles satisfying the GATE criterion of Fig. 9. This is typical of spectra used to determine the mixing of E2 to M1 multipole radiation in the 1.43-MeV γ ray.

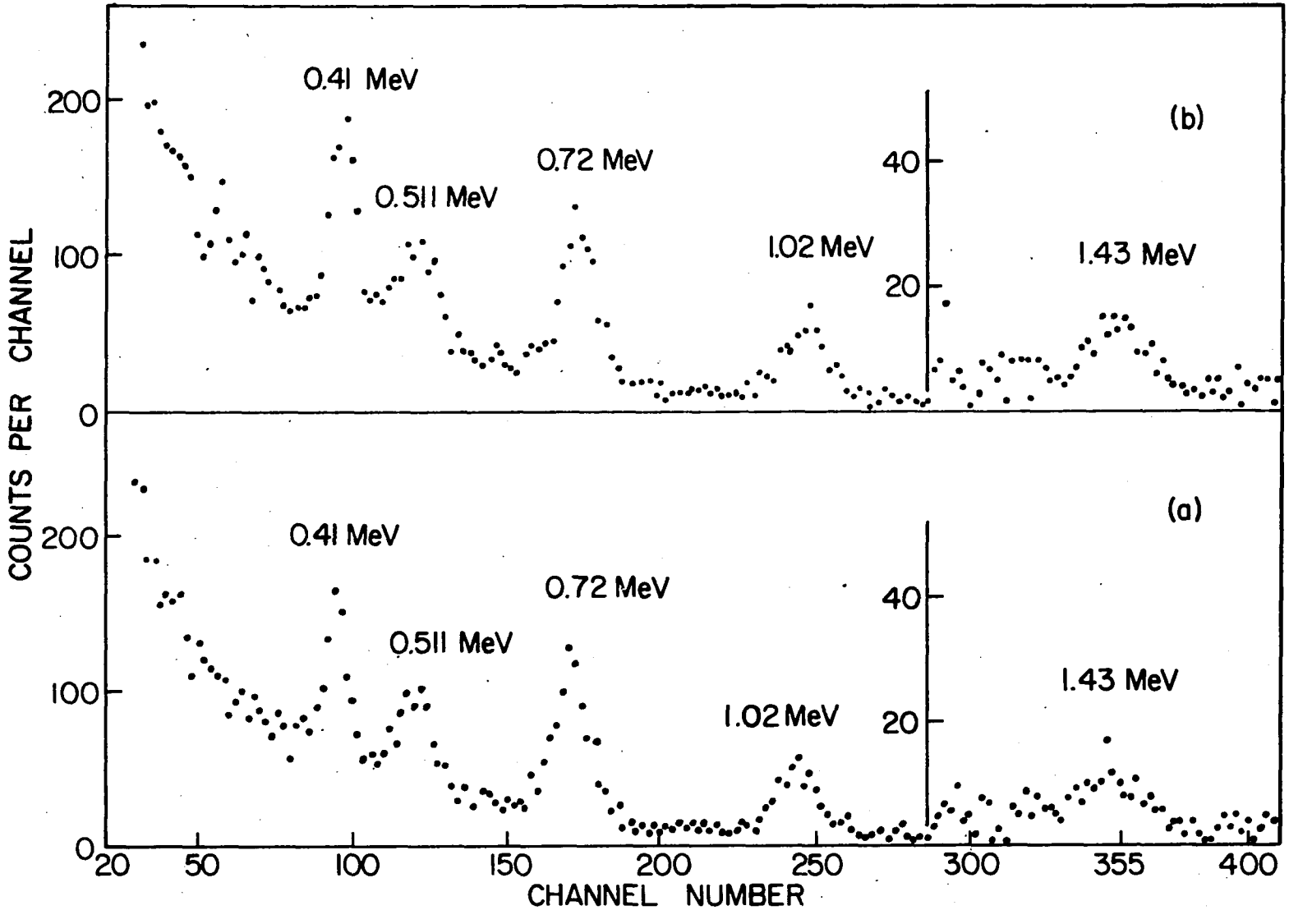
0.41 MeV
0.511 MeV
0.72 MeV
1.02 MeV
1.43 MeV
(b)
(a)
COUNTS PER CHANNEL
CHANNEL NUMBER
200
100
0
40
20
20
50
100
150
200
250
300
355
400

result indicates that there is very little, if any, collective enhancement of the E2 multipole component in this transition.

V. DISCUSSION OF RESULTS

A. Plane-Wave Butler Theory for (^{3}He,α) Reactions

The angular distribution of the α particles from the ^{11}B(^{3}He,α)^{10}B reaction displayed an obvious lack of symmetry about 90° in the center of mass system. Also in some cases, forward peaking was observed. Both these phenomena are characteristic of direct reactions in which the reaction takes place without the formation of an intermediate compound nucleus. We decided to try to fit the angular distribution with a curve derived from direct reaction theory. There are many forms or degrees of approximation of the theory which lead to the calculation of specific angular distributions. In most cases these approximations fall into one of two important categories, the plane wave Born approximation (Butler theory)[21] and the distorted wave Born approximation (DWBA).[22] The Butler theory appeared first and had many successes. The latter differs from the former, as their names imply, in the approximation made about the wave functions of the incident outgoing particles. The Butler theory approximates them with plane waves, while DWBA accounts for the long range distortion by using wave functions obtained from elastic scattering data.

The approximation used to interpret the measured angular distributions is the Butler theory which will be extended to the case of (^{3}He,α) reactions. This approximation is probably not as good as the DWBA for the cases discussed here but is more convenient to use. The effect of using plane waves is to greatly reduce the accuracy of the absolute magnitude of the differential cross section predictions. The reason is that the form of the radial part of the wave function will directly effect the magnitude of the matrix elements. The distortions of the wave functions are caused by central nuclear and coulomb forces, so that the angular part of the wave function will only be affected by the difference in the way non-central components of the nuclear forces are applied. Since non-central components of the nuclear forces are relatively small,[16] the angular part of the wave function is not expected to be affected much by this approximation to the wave functions. The form of the angular distribution is governed by the angular momentum of the nuclear states involved, as well as the energy and spins of all particles. Since the angular information is contained in the angular part of the wave functions, it is expected that the Butler theory will at least predict the shape of the angular distribution. Since all the quantum numbers which angular distributions usually predict are known in

this case the only information that will be obtained from the analysis is whether or not the reaction is direct.

A direct reaction is one which proceeds from an initial configuration (incident particle and target) to a final configuration (product nuclei) directly, without forming an intermediate state which lives long enough to erase any memory of the initial configuration. This is one brief way of defining direct reactions; for more complete treatments of the topics discussed here the reader is referred to a recent survey article[22] and to the references therein. There are two distinct direct processes which could take place in the (^{3}He,α) reaction. In one the ^{3}He ion picks up a neutron as it passes close to the surface of the target nucleus. This is the process which appears to dominate the cases measured here. In the other process the ^{3}He nuclei is absorbed into the target and an α particle is immediately emitted. In order for this exchange process to occur in a direct manner it must be assumed that the α particle existed as a separate entity in the target nucleus. This configuration has a relatively small probability of being present. Backward peaking in the angular distribution is indicative of exchange processes.[23,24] This feature was not observed in the data presented here. The exchange contribution is assumed to be small as might have been predicted[23] and is therefore not discussed further.

Plane wave pick-up theory will be developed for (^{3}He,α) reaction in essentially the same manner Tobocman[25] develops (p,d) pick-up theory. In the first order Born approximation, the differential cross section is given in terms of the wave numbers associated with the incident and outgoing channel by

$$\frac{d\sigma_{ij}}{d\Omega} \propto \frac{k_j}{k_i} \left| A_{ij}(k_i,k_j) \right|^2 , \qquad (27)$$

where i refers to the incident channel and j to the exit channel. The wave number, k is defined in the following manner

$$\vec{k} = \left[\frac{2\mu E}{\hbar^2}\right]^{\frac{1}{2}} \frac{\vec{p}}{|p|} = \frac{\vec{p}}{\hbar} , \qquad (28)$$

where μ is the reduced mass of the two particle system, E is the energy of the system and p is the relative linear momentum. The amplitude A_{ij} is the matrix element

$$A_{ij} = < \varphi_j^+ \, |V_{ji}| \varphi_i^- > , \qquad (29)$$

for the interaction, V_{ji}. The superscripts - and + signify incoming and outgoing particles, respectively. For a plane wave approximation, the wave function may be written in the form

$$\varphi^{+(-)} = \exp\left[+(-)i\vec{k}_p \cdot \vec{r}_{pt}\right] \varphi(t) \, \varphi(p) \qquad (30)$$

where p refers to the incident (exit) particle and t refers to the target (residual) nucleus.

For (^{3}He,α) pick-up reactions let the subscript, β, refer to the incident ^{3}He particle, α, refer to the outgoing α particle and, I, refer to the target nucleus consisting in a core, C, and a neutron, n. Thus the entrance channel wave function is

$$\varphi_i^- = e^{-i\vec{k}_\beta \cdot \vec{r}_{I\beta}} \varphi(i)\ \varphi_\beta\ \varphi_n\ \varphi_C\ , \qquad (31)$$

and the exit channel wave function is

$$\varphi_j^+ = e^{i\vec{k}_\alpha \cdot \vec{r}_{C\alpha}} \varphi(\alpha)\ \varphi_\beta\ \varphi_n\ \varphi_C\ , \qquad (32)$$

where φ_γ is the internal wave function of the particle, γ. For convenience the reaction is pictorially represented in Figure 20 where part (a) depicts the incident channel and part (b) the exit channel.

The Hamiltonian of the system is

$$\begin{aligned} H_{in} &= T_{\beta I} + T_{nC} + V_{nC} + V_{\beta C} + V_{\beta n} \\ H_{out} &= T_{C\alpha} + T_{n\beta} + V_{nC} + V_{n\beta} + V_{C\beta} \end{aligned} \qquad (33)$$

where T_{ab} is the relative kinetic energy of the (a + b) system and V_{ab} is the interaction between a and b. The initial state Hamiltonian is

$$H_i = T_{\beta I} + T_{nC} + V_{nC} \qquad (34)$$

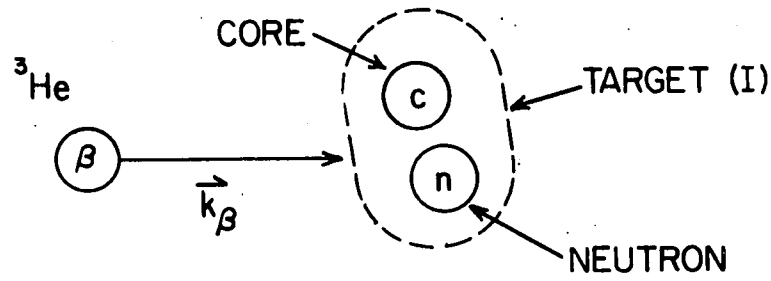

INITIAL STATE

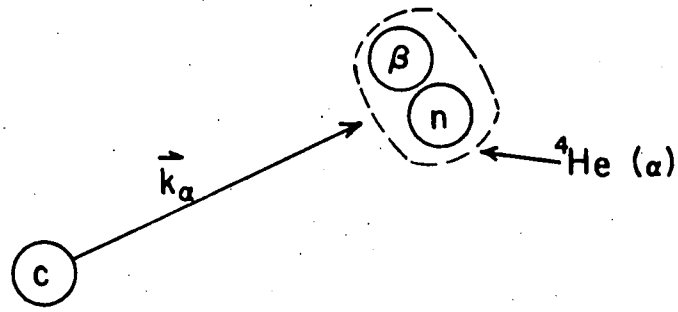

FINAL STATE

Fig. 20. Schematic Diagram of Pick-up Reaction.

and the final state Hamiltonian is

$$H_j = T_{C\alpha} + T_{n\beta} + V_{n\beta} \cdot \qquad (35)$$

The interaction terms for the initial state are $V_{\beta C}$ and $V_{\beta n}$ and for the final state they are $V_{\beta C}$ and V_{nC}. If it is assumed that the core does not interact with the incident ^{3}He particles, the $V_{\beta C}$ is zero. It will also be assumed that all interactions are central. The matrix element may now be written as follows

$$A_{ij} = \langle e^{ik_\alpha \cdot r_{\alpha C}} \varphi_\beta \varphi_n \varphi_\alpha(r_{n\beta}) | V_{\beta n} + V_{nC} | e^{ik_\beta \cdot r_{\beta I}} \varphi_\beta \varphi_n \varphi_C \varphi_I(r_{nC}) \rangle$$

$$= \iint dr_{\beta I} dr_n \; e^{-ik_\alpha \cdot r_{C\alpha}} \varphi^*_\alpha(r_{n\beta})(V_{n\beta} + V_{nC}) e^{ik_\beta \cdot r_{I\beta}} \varphi_I(r_{nC}) \,, \qquad (36)$$

where the fact that $\langle \varphi_\gamma | \varphi_\gamma \rangle = 1$ was used. It is convenient to make a change of variables at this point from $r_{I\beta}$ and $r_{C\alpha}$ to $r_{n\beta}$ and r_{nC} by making use of the following relations which are vectorially represented in Figure 21

$$\vec{r}_{I\beta} = \vec{r}_{n\beta} - \frac{m_C}{m_I} \vec{r}_{n\beta} \qquad (37)$$

$$\vec{r}_{C\alpha} = -\vec{r}_{nC} + \frac{m_\beta}{m_\alpha} \vec{r}_{n\beta} \qquad (38)$$

where m_a is the mass of the a^{th} nucleus. Making these substitutions the matrix element becomes

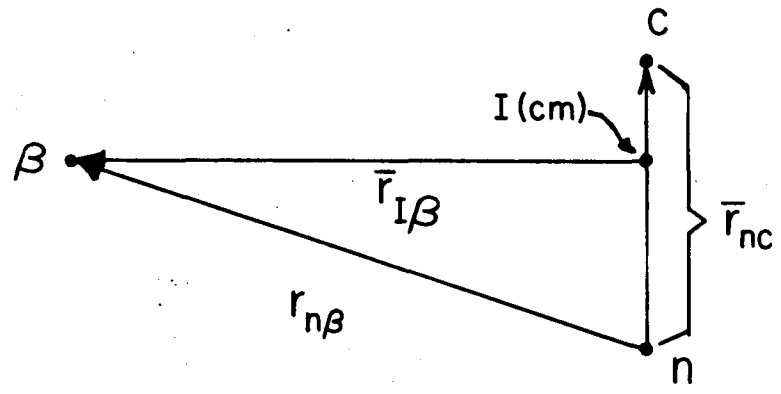

INITIAL STATE

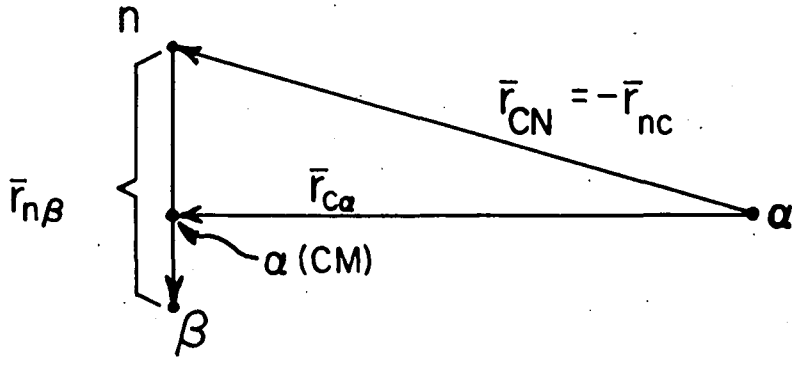

FINAL STATE

Fig. 21. Coordinate Diagram

$$A_{ij} = \int dr_{n\beta} \int dr_{nC}\; e^{-i\varkappa \cdot r_{nC}}\; \varphi_I^*(r_{nC})\left[V(r_{nC}) + V(r_{n\beta})\right]$$

$$\times\; e^{i\nu \cdot r_{n\beta}}\; \varphi_\alpha(r_{n\beta}) \qquad (39)$$

where $\varkappa$ and ν are defined as follows

$$\vec{\varkappa} = \left[\vec{k}_\alpha - \frac{m_C}{m_I}\,\vec{k}_\beta\right] \qquad (40)$$

and

$$\vec{\nu} = \left[\vec{k}_\beta - \frac{m_\beta}{m_\alpha}\,\vec{k}_\alpha\right] . \qquad (41)$$

Although $\vec{\varkappa}$ and $\vec{\nu}$ were obtained from a straight forward change of variables they have special physical significance; $\varkappa$ is the momentum transferred to the ^{10}B core and ν is the momentum transferred to the ^{3}He nucleus. From the definition of these quantities it is seen that their values depend on the relative directions of $\vec{k}_\alpha$ and $\vec{k}_\beta$. It is through these momentum transfers that the cross section obtains its angular dependences. This fact is apparent in the expression for the cross section derived below. The interactions $V(r_{n\beta})$ and $V(r_{nC})$ are eliminated by using Schroedinger's equation which can be written in the form

$$V(r)\varphi(r) = \frac{\hbar^2}{2\mu}\left(\nabla^2 - \omega^2\right) , \qquad (42)$$

where ω is defined in terms of the binding energy, BE, of the system by

$$\omega^2 = \frac{2\mu(BE)}{\hbar^2} . \qquad (43)$$

Making use of equation (42) the integrations in equation (39) can be simplified in the following manner

$$\int dr\ e^{-ik\cdot r}\ V(r)\varphi(r) = \int dr\ e^{-ik\cdot r}\ \frac{\hbar^2}{2\mu}\ (\nabla^2 - \omega^2)\varphi(r)$$

$$= -\frac{\hbar^2}{2\mu}\left[k^2 + \omega^2\right] \int dr\ e^{-ik\cdot r}\ \varphi(r). \qquad (44)$$

The matrix element can now be written in the form

$$A_{ij} \propto \left[\frac{\kappa^2 + k_\alpha^2}{\mu_{n\beta}} + \frac{\nu^2 + k_I^2}{\mu_{nC}}\right] \int e^{-i\kappa\cdot r_{nC}}\ \varphi(r_{nC})dr_{nC}$$

$$\times \int e^{i\nu\cdot r}\ \varphi_\alpha(r_{n\beta})dr_{n\beta} . \qquad (45)$$

The wave functions $\varphi_\alpha(r_{n\beta})$ and $\varphi_I(r_{nC})$ are assumed to represent states of sharp angular momentum so that they may be written expressly in terms of the orbital angular momentum, ℓ, and its projection, m

$$\varphi_I(r_{nC}) = \varphi_I^{\ell}(r_{nC})\ y_\ell^m\ (\Omega_{nC}) , \qquad (46)$$

and

$$\varphi_\alpha(r_{n\beta}) = \varphi_\alpha^{\ell'}(r_{n\beta})\ y_{\ell'}^{m'}\ (\Omega_{n\beta}) \qquad (47)$$

where $y_\ell^m\ (\Omega_{n\beta})$ are spherical harmonics. At this point it is convenient to define a function which occurs often in direct reaction theory

$$F^A_{\ell m}(k) = \int d\vec{r}\; e^{ik\cdot r}\; \varphi^{\ell}_A(r)\; y^m_{\ell}(\Omega)\ . \qquad (48)$$

If $e^{-ik\cdot r}$ is expanded in terms of spherical harmonics it has been shown that[25]

$$F^A_{\ell m}(k) = 4\pi i^{\ell}\; y^m_{\ell}(\Omega) \int_o^{\infty} dr\; r^2\; j(kr)\varphi^{\ell}_A(r)\ . \qquad (49)$$

The matrix element expressed in terms of $F^A_{\ell m}(k)$ is

$$A_{ij} \propto \left[\frac{\varkappa^2 + k^2_{\alpha}}{\mu_{\alpha}} + \frac{\nu^2 + k^2_I}{\mu_I}\right] F^{\alpha}_{\ell' m'}(\varkappa)\; F^I_{\ell m}(\nu)\ . \qquad (50)$$

If the reference axis for the coordinates used in $F^A_{\ell m}(k)$ is chosen to coincide with the argument, k, then the factor $y^m_{\ell}(\Omega_k)$ will be given by

$$y^m_{\ell}(0) = \delta_{m0}\,\frac{4\pi}{2\ell+1}\ . \qquad (51)$$

The integral in $F^A_{\ell m}(k)$ can be approximated in two ways. One way is to impose a surface postulate which requires all the interaction to take place outside a sphere of radius, R, about the target nucleus. The effect of this approximation is to place a lower cutoff on the integral. The integral can then be evaluated since the wave function, φ, outside the nuclear radius is known to be proportional to a Hankel function.[26] With this approximation the function $F^A_{\ell}(k)$ becomes

$$F_\ell^A(k) \propto \frac{1}{(k^2+\omega_A^2)} \left[\frac{d}{dR}\, j_\ell(kR) - j_\ell(kR)\frac{d}{dR}\, \ell n\, h_\ell^{(1)}(ikr)\right]. \quad (52)$$

This method is employed in what is usually called the Butler theory. An alternate method, first suggested by Bhatia et al.,[27] is to observe that, because of the $(kR)^2$-dependence of the Bessel function and the exponentially decreasing dependence of φ on r, there will occur a sharp maximum in the integrand at some radius, R, which will be called the radius of the nuclear surface. The integral is then approximated by the value of the integrand at that surface as follows

$$F_\ell^A(k) \simeq \frac{R^2}{W_A^2}\, \varphi_A^\ell(R)\; j_\ell(kR)\ . \quad (53)$$

These two approaches result in the same distribution. However, the former will usually require a smaller radius than the latter to fit the same data.

Because of its simplicity, the latter approximation was made through the analysis of the present experiments. No attempt has been made to retain factors which are independent of direction because the absolute magnitude of the cross section is of questionable value in a plane-wave approximation for incident energies lower than the coulomb barrier.

The amplitude may now be written as

$$A_{ij} \propto \left[\frac{\varkappa^2 + \omega_I^2}{\mu_{nc}} + \frac{\nu^2 + \omega_\alpha^2}{\mu_{n\beta}}\right] j_\ell(\varkappa R_I)\; j_{\ell'}(\nu R_\alpha) \;, \qquad (54)$$

and therefore the differential cross section becomes

$$\frac{d\sigma}{d\Omega} \propto \left[\frac{\varkappa^2 + \omega_I^2}{\mu_{nc}} + \frac{\nu^2 + \omega_\alpha^2}{\mu_{n\beta}}\right]^2 j_\ell^2(\varkappa R_I)\; j_{\ell'}^2(\nu R_\alpha) \;. \qquad (55)$$

The value of ℓ is determined by the state in which the neutron moves about the core. For ^{11}B the shell model predicts it to be a $p_{3/2}$ state, therefore $\ell = 1$. Similarly the value of ℓ' is determined by the state in which the neutron moves about the ^{3}He core. Here the shell model predicts this state to be $s_{\frac{1}{2}}$, therefore $\ell' = 0$.

The angular distributions of the α particles from the formation of the first three states in ^{10}B were fit with this theory by calculating the distribution, varying R_I and R_α to obtain the best fit. Figure 22 shows the distribution of the α particles from the formation of the ground state; the points are the experimental data and the solid line is the theoretical fit. The best fit was obtained for $R_\alpha = 1.5 \times 10^{-13}$ cm and $R_\beta = 4.1 \times 10^{-13}$ cm. The shape appears to be fairly well predicted by the plane-wave theory although the relative magnitude predictions are not very good as was expected. The conclusion is that direct

Fig. 22. Angular Distribution of α_0. The angular distribution of α particles leading to the ground state in ^{10}B from the reaction $^{11}B(^{3}He,\alpha)^{10}B$ is plotted. The points are the experimental data plotted to an arbitrary scale with a relative uncertainty of 5%. The solid curve is the Butler plane wave pick-up prediction with $R_\alpha = 1.5$ fermis, $R_{^{11}B} = 4.1$ fermis and $\ell = 1$.

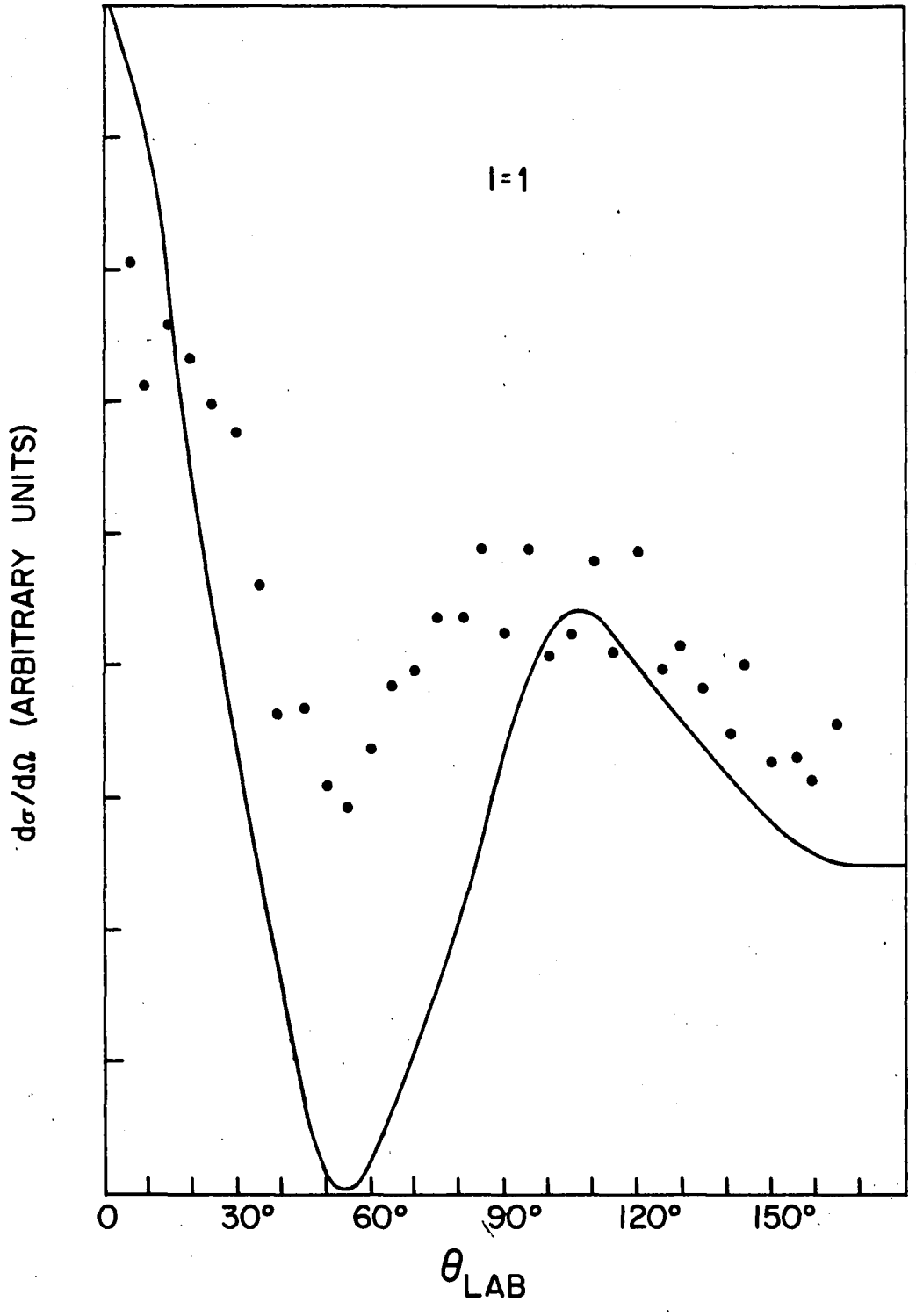
l=1
dσ/dΩ (ARBITRARY UNITS)
0
30°
60°
90°
120°
150°
θLAB

interactions are present in the reaction. In making this conclusion it should be pointed out that there are other nuclear processes which do have non-symmetric distribution. Such a process is one in which the compound nucleus is formed but decays after one or two internal collisions rather than many as is assumed in the statistical approach. Here the probability of such a process is assumed to be small compared to the probability of a direct interaction at the surface. Thus, the angular dependence is assumed to receive its dominate features from the direct process.

In Figure 23, the distribution of α particles from the formation of the 0.72 state in ^{10}B is shown. Again the points are the experimental data and the line is the prediction of the plane-wave theory. The radii that gave the best fit are $R_\alpha = 1.5 \times 10^{-13}$ cm and $R_\beta = 4.3 \times 10^{-13}$ cm. The predicted shape appears to fit the data; although, again, the magnitudes do not agree everywhere. Therefore, it is assumed that direct interactions are present in this reaction also.

In Figure 24 the distribution of the α particles from the formation of the 1.74-MeV state is shown. In this case the shape of the distribution could only be fit with the theoretical prediction if the value for ℓ was taken to be 0, rather than 1. That is, if the theory applies the neutron is removed from an inner $s_{\frac{1}{2}}$ shell rather than the outer $p_{3/2}$ shell. No reason for this can be given although

Fig. 23. Angular Distribution of α_1. The angular distribution of α particles leading to the 0.72-MeV state in ^{10}B from the reaction $^{11}B(^{3}He,\alpha)^{10}B$ is plotted. The points are the experimental data plotted to an arbitrary scale with a relative uncertainty of 5%. The solid curve is the Butler plane wave pick-up prediction with R_α = 1.5 fermis, $R_{^{11}B}$ = 4.1 fermis and ℓ = 1.

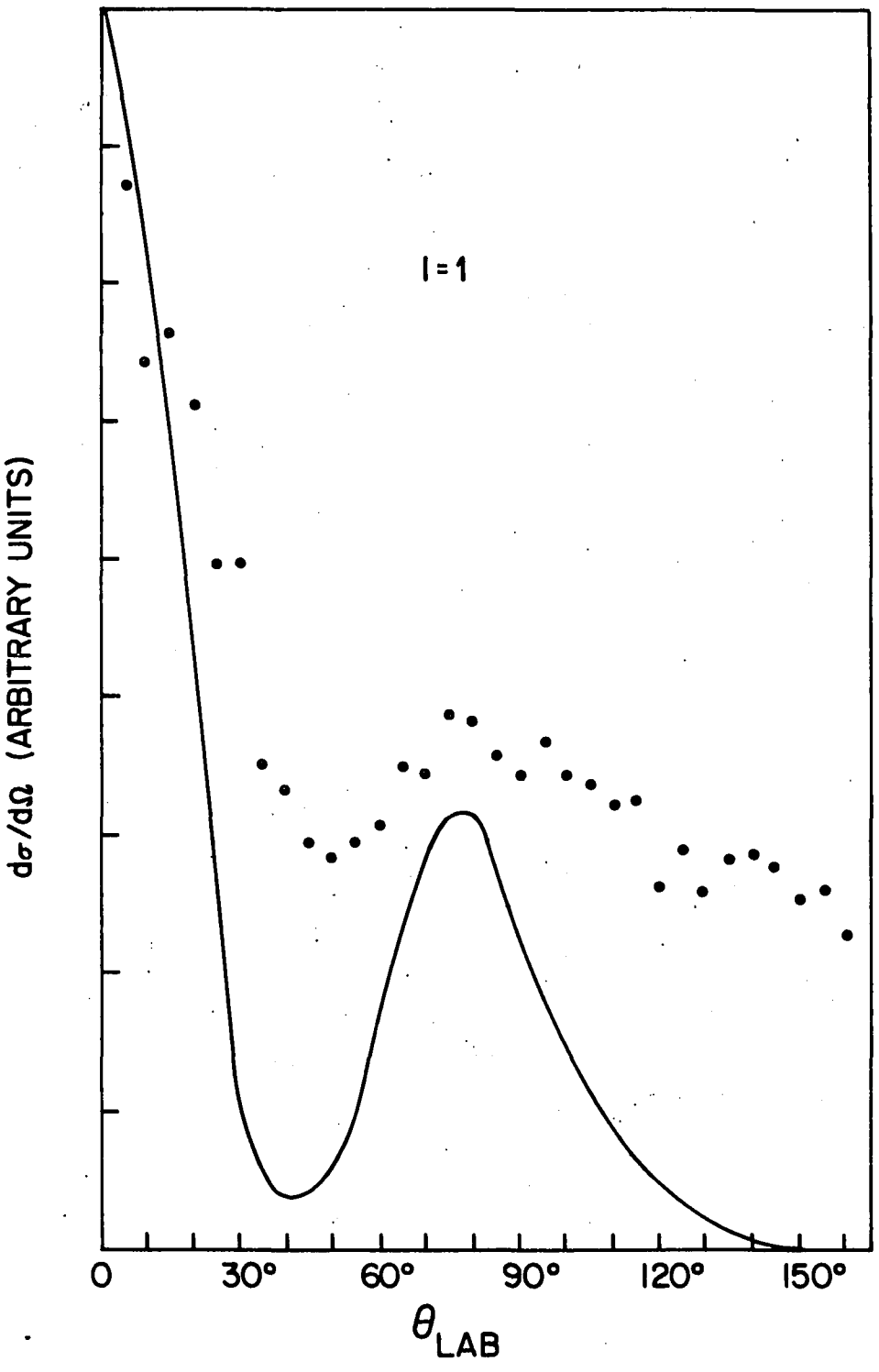
l=1
dσ/dΩ (ARBITRARY UNITS)
0
30°
60°
90°
120°
150°
θLAB

Fig. 24. Angular Distribution of α_2. The angular distribution of α particles leading to the 1.74-MeV state in ^{10}B from the reaction $^{11}B(^{3}He,\alpha)^{10}B$ is plotted. The points are the experimental data plotted to an arbitrary scale with a relative uncertainty of 5%. The solid curve is the Butler plane wave pick-up prediction with $R_\alpha = 1.5$ fermis, $R_{^{11}B} = 3.9$ fermis and $\ell = 0$.

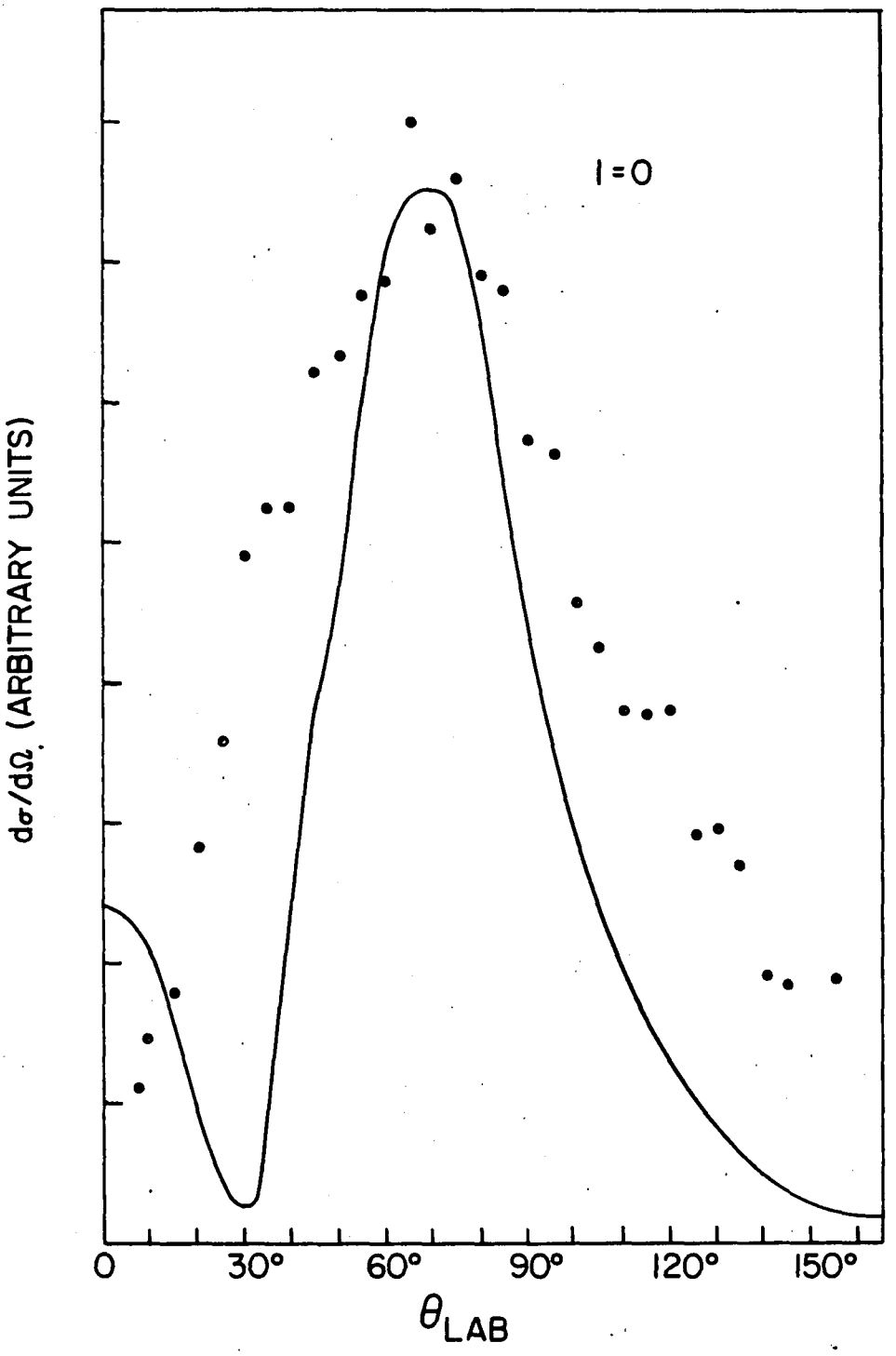
I=0
dσ/dΩ (ARBITRARY UNITS)
0
30°
60°
90°
120°
150°
θLAB

it should be pointed out that this final state has isotopic spin T = 1 whereas all the others have T = 0. Attempts to fit the data with $\ell = 1$ were made and some degree of success was obtained if the value of the radius of the ^{11}B nucleus was assumed to be about twice what was observed in the other cases. This was not thought to be physically meaningful. Also, the possibility that the distribution is really symmetric about 90° was investigated. Two separate measurements of the distribution were made for $E_{^3He} = 2.15$ MeV besides the measurements at 1.0 and 1.8 MeV. All results indicated that the peak observed in the distribution was not at 90° in the center of mass system. This is clear in Figure 24 where the points are the experimental data and the line is the theoretical prediction with $\ell = 0$. The values of the radii which best fit the data are $R_\alpha = 1.5 \times 10^{-13}$ cm and $R_{^{11}B} = 3.9 \times 10^{-13}$ cm. Direct reaction mechanism is assumed to be present in this case although the reason for the removal of an $s_{\frac{1}{2}}$-neutron is not clear.

The angular distribution of the α particles from the formation of the 2.15-MeV state appeared to be symmetric about 90°. This can be seen in Figure 25 where the points represent the experimental data. Because of this symmetry the data were fit with the first two even Legendre polynomials. The fit is indicated by the solid line in the figure and appears to support the contention of symmetry about 90°. The exact function used is

Fig. 25. Angular Distribution of α_3. The angular distribution of α particles leading to the 2.15-MeV state in ^{10}B from the reaction $^{11}B(^{3}He,\alpha)^{10}B$ is plotted. The points are the experimental data plotted to an arbitrary scale with a relative uncertainty of 5%. The solid curve is the symmetric function $W(\theta) = I(1 + 1.25\ P_2\ (\cos\ \theta))$.

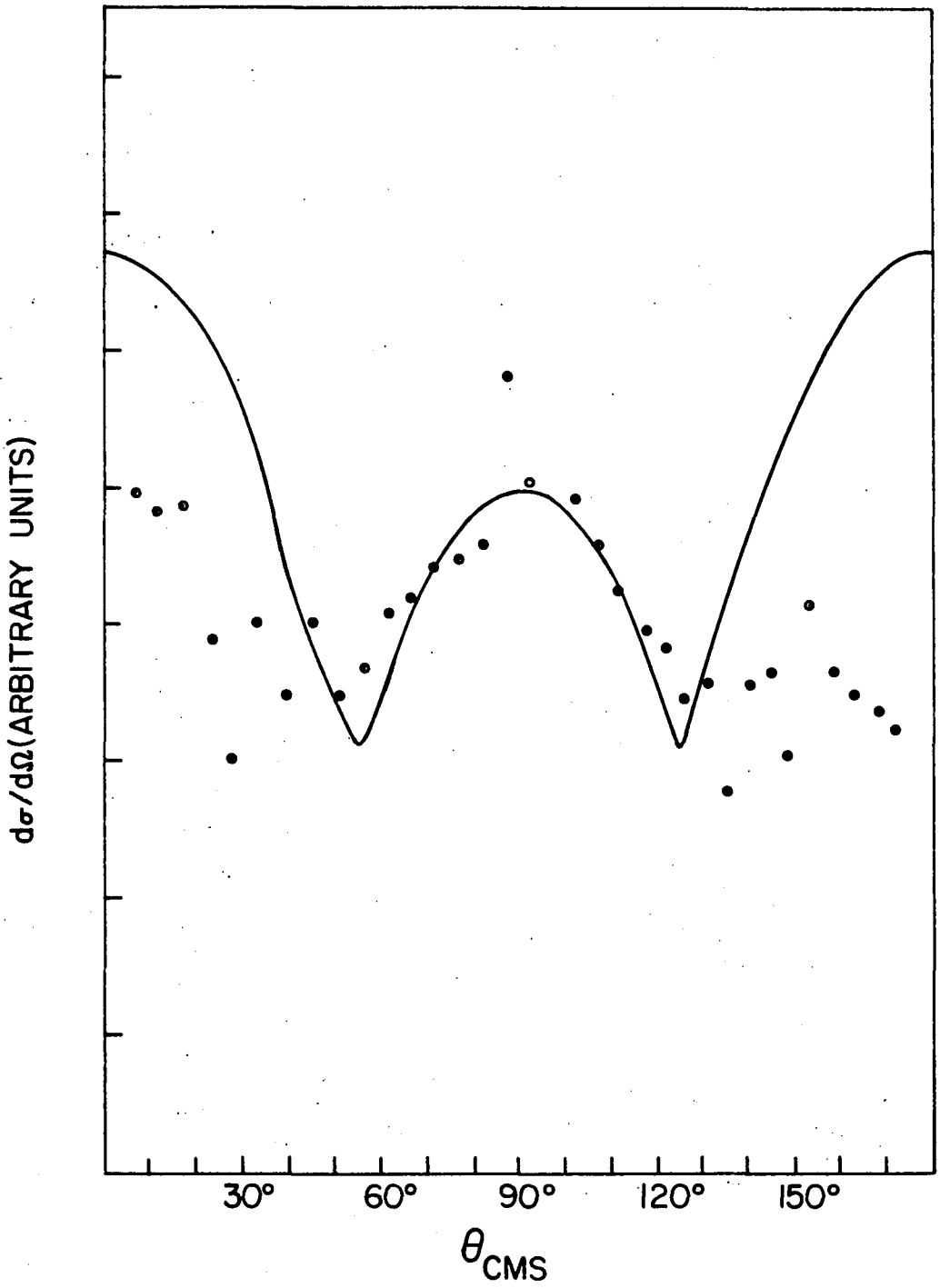
dσ/dΩ(ARBITRARY UNITS)
30°
60°
90°
120°
150°
θCMS

$$W(\theta) = I[1 + 1.125\ P_2(\cos\ \theta)]\ . \qquad (56)$$

Because of this symmetry it was concluded that the reaction leading to this state proceeds through a compound nucleus most of the time.

B. Comparison of Mean Lives to Shell Model Predictions

In this section the measured values of mean lives will be compared with several theoretical predictions of these quantities.

In general a γ-ray transition probability (radiative width) is written

$$\Gamma \propto | < \psi_f^* | \Omega | \psi_i > |^2 \qquad (57)$$

where ψ_i and ψ_f are the wave functions of the initial and final states, respectively. The operator, Ω, describes the electromagnetic interaction and can be expanded in a series of terms each of which is associated with either an electric or magnetic transition of definite multipolarity. This total radiative width is related to the mean life by the expression $\Gamma\tau = \hbar$.

Weisskopf[28] has calculated values for radiative widths by using single particle wave functions. He assumes that the radial part of the wave function is constant inside the nuclear matter and that the single particle moves in a spherical potential with well defined angular momentum. The

radiative widths determined under these assumptions will, in general, be larger than if more realistic wave functions were used. For this reason they are called Weisskopf limits and are often used as a basis for comparing measured mean lives.

In Table III the results of our experiments are compared with the Weisskopf limits. The first two columns define the transition, the third column gives the multipolarity of the transition and the fourth column gives the change in isotopic spin. The fifth column lists the Weisskopf limit for each transition which is to be compared with the experimentally determined widths listed in the sixth column. The last column lists the ratio of measured widths to Weisskopf limits. Wilkinson[29] has compiled other available data and has made a similar comparison. He finds that, for M1 transitions, experimental widths are about 1/7 times the Weisskopf limit. However, for self-conjugate nuclei, of which ^{10}B and ^{14}N are examples, there is a selection rule proposed by Morpurgo[30] which inhibits M1 transitions for which the change in isotopic spin is not $\Delta T = \pm 1$. He suggests that transitions violating this rule should be inhibited by a factor of 100, so that the associated width should be about 1/700 times the Weisskopf limit. Finally Wilkinson finds that most E2 transitions are about 5 times the Weisskopf limits.

TABLE III

Comparison of Radiative Width with Weisskopf Estimates

Nucleus	Transition	Multipolarity	ΔT	Weisskopf[28] Estimate, Γ_W (10^{-3} ev)	Measured Value Γ_m (10^{-3} ev)	Γ_m/Γ_W
^{10}B	3.58 → 0.72	M1	0	700	3.0	0.0043[a]
^{10}B	3.58 → g.s.	M1	0	1200	0.70	0.0058[a]
^{10}B	2.15 → 1.74	M1	+1	2.5	0.04	0.016
^{10}B	2.15 → 0.72	M1	0	80	0.05	0.0062[a]
^{10}B	2.15 → g.s.	E2	0	.06	0.04	.6
^{10}B	1.74 → 0.72	M1	-1	400	3.46	0.0086
^{14}N	3.95 → 2.31	M1	+1	150	> 25.0	> 0.166
^{14}N	3.95 → g.s.	M1	0	3000	> 1.0	> 0.00033[a]
^{14}N	2.31 → g.s.	M1	-1	700	8.0	0.012

[a]These transitions violate the isotopic spin selection rule for self-conjugate nuclei.

The results of the comparison indicates that the radiative widths measured here are similar to other widths measured for other nuclei. Of particular interest is the fact that the isotopic spin selection rule apparently holds. These measurements provide the most extensive test of this selection rule to date.

A more realistic comparison of transition probabilities can be made with predictions calculated from the shell model with intermediate coupling. The nuclear shell model[33] has been very successful in describing ground state properties of nuclei. When the model is applied to excited states, complications occur which require extension of the model. One such complication is the question of how to couple the odd nucleons in an odd-odd nucleus. If, in ^{14}N, the holes in the p-shell are assumed to behave as particles, the nuclei ^{10}B and ^{14}N are both examples of this case. These two nucleons interact with the core, that is, the filled shells, through an average central potential. Also they interact with each other through two distinct potentials. One is the spin-orbit interaction, $a(\vec{l}\cdot\vec{s})$, and the other is a nuclear exchange interaction, K, which depends on their separation. Over the range of nuclei filling the p-shell, a/K will vary as a since K is not expected to change much.[34] Strictly speaking LS coupling applies for $a/K = 0$ and j-j coupling applies for $a/K = \infty$. However, these different

coupling schemes describe the nucleus reasonably well if $a/K \leq 1$ or if $a/K \geq 5$, respectively.

The intermediate coupling model[35-38] applies for the cases where $1 \leq a/K \leq 5$, that is, where neither extreme coupling scheme applies. In this model the intermediate wave functions are obtained[38] in terms of either LS or j-j wave functions. The base wave functions are calculated using either $a/K = 0$, or ∞. The spin-orbit coupling is then included in the Hamiltonian as a function of the parameter a/K. The Hamiltonian is diagonalized by a transformation which is in turn used to generate the intermediate coupling wave functions in terms of the base functions. These intermediate wave functions depend on a/K and are used to calculate the matrix elements in the expression for the transition probabilities. This calculation has been carried out for ^{10}B by Kurath[34] for several values of a/K. His results are expressed in terms of transition strengths, Λ, which are proportional to the radiative widths with the dependence on the γ-ray energy taken out. Explicitly for M1 transitions, Λ is defined as

$$\Lambda(M1) = \Gamma(M1)/2.76 \times 10^{-3} E_\gamma^3 \qquad (58)$$

and for E2 transitions as

$$\Lambda(E2) = \Gamma(E2)/8.02 \times 10^{-8} E_\gamma^5 \qquad (59)$$

where E_γ is the γ-ray energy. Kurath's calculations are compared with experimental results in Table IV. The first column specifies the transition, the second column gives the multipolarity of the transition. The next six columns list calculated values of the transition strengths for six values of a/K. The last column lists the experimentally determined transition strengths. For transitions in which both M1 and E2 are allowed, only the M1 transition is listed since in all cases the measured mixing ratios[32] indicated that the intensity of the E2 component was less than 20% of the total intensity. The branching ratios used to determine the radiative width of various transitions are those[18] shown in Figure 2.

For the M1 transitions the experimental values of the transition strengths indicate that $1.5 \leq a/K \leq 3.0$. These values of a/K do not agree with values which, according to Kurath[34], are necessary in order that the observed energy level scheme of ^{10}B be predicted. That is, a/K must be between 4 and 5 if energy levels, which are identified by their spin, parity and isotopic spin, are to occur in the order observed. The fact that a/K might be lower than Kurath predicts has been suggested before by Warburton et al.[31] They measured the branching ratio of decays of the 3.58-MeV state in ^{10}B to the 0.72-MeV state and to the ground state to be (4.2:1). Their value of this quantity

TABLE IV

Transition Strengths for Transitions in ^{10}B

Transition	Multi-polarity	a/K 1.5	3.0	4.5	6.0	7.5	Emperical Values
3.58 → 0.72	M1	0.000	0.052	0.060	0.051	0.044	0.045
3.58 → g.s.	M1	0.005	0.044	0.062	0.069	0.072	0.0059
2.15 → 1.74	M1	0.02 ←→[a]	9.22	13.27	12.27	11.31	0.18
2.15 → 0.72	M1	0.001	0.135	0.046	0.039	0.038	0.0065
2.15 → g.s.	E2	0.092	0.638	0.503	0.451	0.428	10.7
1.74 → 0.72	M1	62.8 ←→[a]	29.7	14.10	15.70	18.40	1.18

[a]The symbol ←→ means the matrix element changes sign between these entries, i.e., A vanishes in this interval.

agrees best with the intermediate coupling prediction for $a/K = 1$, although the best agreement was poor. This ratio is consistent with the γ-ray intensities that we observed. Therefore, it appears that the intermediate coupling model should be re-examined.

The experimental transition strength of the E2 ground state transition from the 2.15-MeV states appears much greater than the intermediate coupling model predicts. Such enhanced E2 transitions are not uncommon and are usually attributed to collective effects. The shell model calculations discussed here do not account for core excitation, that is, the excitation of nucleons in closed subshells. Such excitations would involve many nucleons so that in their decay larger angular momentum transfers are more likely than for single nucleon excitations. This situation would tend to enhance the higher multipole transitions, such as E2.

The strength for transitions in ^{14}N calculated from the intermediate coupling formation are not available. However, such strengths for extreme j-j coupling and for LS coupling have been computed by Warburton and Pinkston.[39] Their results for the states measured here are compared with these measurements in Table V. The first two columns identify the transition and its multipolarity. The next column gives the radiative width determined from the mean life and the branching ratios[40] given in Figure 17. The

TABLE V

Transition Strengths in ^{14}N

Transition	Multi-polarity	Λ			
		Experimental Value	a(j-j)	b(LS)	c(LS)
2.31 → 0	M1	0.27	2.45	0.46	0.70
3.95 → 2.31	M1	> 2.10	7.88	13.1	11.3
3.95 → 0	M1	> 0.0058	0.032	0.0029	0.0033
5.10 → 0	(E1,M2,E3)				

last three columns give the transition strengths calculated from the extreme coupling schemes. Column (a) lists the results if j-j coupling[39] is assumed, column (b) and (c) list results if LS coupling is assumed. These latter two columns differ in that for the column (b) the wave functions of Elliot[41] were used in the calculations and for column (c) those of Visecher and Ferrell[42] were used. These wave functions differ in the choice of force parameters used to derive them.

The experimental results indicate that LS coupling applies for the 2.31-MeV state. The limit put on the mean life of the 3.95 MeV indicates that LS coupling predicts transition strength that are too small. Therefore LS coupling does not apply to this state, whereas j-j coupling could apply.

Unfortunately little was learned from the limit placed on the mean life of the 5.10-MeV state. The ground state transition is unique because it has significant components of three multipole radiation (E1, M2, E3), as was shown by Blake et al.[43] The measured limit indicates only that the E1 transition is inhibited, presumably by the isotopic spin selection rule[29] $\Delta T = \pm 1$. That the E3 is enhanced could not be determined.

VI. SUMMARY AND CONCLUSION

The mean lives of the 3.58-, 2.15- and 1.74-MeV states in ^{10}B and the 2.31-MeV state in ^{14}N were measured and limits were put on the mean lives of the 5.10- and 3.95-MeV states in ^{14}N by the Doppler-shift attenuation method. The states were produced using the reactions $^{11}B(^{3}He,\alpha)^{10}B$ and $^{12}C(^{3}He,p)^{14}N$. The results of these measurements are listed in Table II. In the employment of this method the kinematics of the reactions were fixed by observing γ radiation in coincidence with particles emitted in a fixed direction in all cases but for the 5.10-MeV state in ^{14}N.

These results are compared with predictions made from the shell model. The ^{10}B data are compared in Table IV with predictions made from the independent particle model with intermediate coupling. It is found that the coupling parameter, a/K, must lie in the range 1.5 to 3.0 in order to obtain agreement with the experimental results. These values disagree with those which give the observed energy level scheme. A thorough examination of the theory is needed in order to explain the discrepancy.

In Table V the ^{14}N data are compared with predictions made from the independent particle model with extreme

j-j and LS coupling schemes. It appears that LS coupling correctly predicts the mean life of the 2.31-MeV state but not that of the 3.95-MeV state. The experimental results for the 5.10-MeV state are not sufficient to allow any positive conclusions to be made from them.

For completeness all the mean-life data are compared in Table III to predictions made from the single particle model by Weisskopf. The predictions disagree with the experimental results by a factor of 10 which is not unexpected because of the approximations in the model. The isotopic spin section rule, $\Delta T = \pm 1$, for M1 transitions in self-conjugate nuclei appears to apply for the cases studied.

The angular distributions of α particles from the formation of the first four states in ^{10}B by the reaction $^{11}B(^{3}He,\alpha)^{10}B$ were measured. The results are shown in Figures 10, 11 and 12. These distributions were fit with a curve predicted by an extension of the plane-wave Butler theory for pick-up reactions. The comparisons are shown in Figures 22, 23 and 24. The theoretical curves agree reasonably well with the observed distribution. It is therefore concluded that the reaction proceeds in a direct manner in all cases except for the formation of the 2.15-MeV state. In this case the reaction appears to proceed through a compound nucleus.

Finally the mixing of E2 and M1 multipole radiations in the 1.43-MeV transition from the 2.15-MeV state to the 0.72-MeV state in ^{10}B was measured. An angular correlation technique was used to determine that the mixing ratio is $|x| \leq 0.07$. This result indicates that there is very little, if any, collective enhancement of the E2 multipole component in that transition.

APPENDIX A

In the Doppler-shift attenuation method the assumption is made that the velocity measured is the average velocity defined in an exact manner by

$$\overline{v} = \int_0^{v_0} v\, f(v)\, dv \ , \qquad \text{(A-1)}$$

where $f(v)$ is the normalized distribution of the velocities. The velocity that is actually measured in the experiment is that velocity associated with the maximum of the observed γ-ray peak. If the observed peak for monoenergetic γ rays is assumed to be gaussian[44] in energy, the shape of a peak from γ rays with a distribution in energy, $f[v(E)]$ can be found by folding this distribution with the gaussian resolution function in the following manner

$$N(E) = \int_{-\infty}^{\infty} e^{\frac{-(E-E')^2}{\sigma^2}} f[v(E')]dE' \ , \qquad \text{(A-2)}$$

where σ is the half-width of the gaussian at 1/e of its maximum applitude. In order to find the maximum of N(E) this equation is differentiated and set equal to zero, giving the following equation for E_m, the energy at which the peak occurs

$$E_m = \frac{\int_{-\infty}^{\infty} E\, e^{-\frac{(E_m - E')^2}{\sigma^2}} f[v(E')] \frac{dv}{dE}\, dE}{\int_{-\infty}^{\infty} e^{-\frac{(E_m - E')^2}{\sigma^2}} f[v(E')] \frac{dv}{dE}\, dE} . \qquad \text{(A-3)}$$

This equation cannot be solved exactly since $f(v)$ is not an analytic function but rather decays from some maximum, v, in an almost exponential fashion to v = 0 where it has a discontinuous jump. However, certain features of the equation can be pointed out. First as the resolution function widens, that is, as σ increases, E_m approaches the average energy $\bar{E}$ which is associated with the average velocity, since they have the same distribution. Also if the distribution $f(v(E))$ is symmetric about E_m, then E_m will correspond to the average energy. In the present experiment, σ is of the order of the range in E for which $f(v(E))$ is non-zero, not large enough to say the gaussian is almost constant corresponding to poor resolution and not small enough that the gaussian could be approximated by a delta function.

In order to get an idea as to how much E_m can be expected to differ from $\bar{E}$, an extreme, but analytic, $f(v(E))$ was used to in the expression for E_m, namely

$$\frac{dv}{dE} f(v(E)) = \frac{4}{E_a} \left(\frac{E}{E_a}\right)^3 \qquad 0 \le E \le E_a \qquad \text{(A-4)}$$

$$= 0 \qquad \text{otherwise.}$$

Here E_a is the maximum energy corresponding to full Doppler shift. This distribution is very non-symmetric about the average energy corresponding to about the worst case that will be encountered experimentally. In order to perform the integration in closed form the gaussian resolution function was approximated by the first two terms in its expansion, assuming, for simplicity, $\sigma = E_a$

$$g(E_m - E') = 1 - \frac{(E_m - E)^2}{E_a^2} . \qquad (A-5)$$

This function is sharper than the gaussian and so represents a worse case than exists in the experiment.

Substituting these functions in equation (A-3) and performing the integration it is found that E_m is within 1% of the average energy. Since this is the worst case it can be assumed that the maximum in the peak will be

$$E_m = \bar{E}(1 \pm 0.01) . \qquad (A-6)$$

This is well within the accuracy at which the peak can be measured. So that the association of the γ-ray peak with the average velocity is justified.

LIST OF REFERENCES

1. S. Devons, G. Manning and D. St. P. Banbury, Proc. Phys. Soc. (London) A68, 18 (1955).

2. A. E. Litherland, M. J. L. Yates, B. M. Hinds, and D. Eccleshall, Nucl. Phys. 44, 220 (1963).

3. E. K. Warburton, D. E. Alburger and D. H. Wilkinson, Phys. Rev. 129, 2180 (1963).

4. A. E. Litherland and A. J. Ferguson, Can. J. Phys. 39, 788 (1961).

5. E. K. Warburton, J. W. Olness, D. E. Alburger, D. J. Bredin and L. F. Chase, Jr., Phys. Rev. 134, B338 (1964).

6. L. C. Biedenharn, in Nuclear Spectroscopy, edited by F. Ajzenberg-Selove (Academic Press Inc., New York, 1960), Part B, pp. 732-810.

7. G. Dearnaley, Rev. Sci. Instr. 31, 167 (1950).

8. D. I. Porat and K. Ramavataram, Proc. Phys. Soc. (London) 77, 97 (1961).

9. D. I. Porat and K. Ramavataram, Proc. Phys. Soc. (London) 78, 97 (1961).

10. American Institute of Physics Handbook, McGraw-Hill Book Company, Inc., New York, 1957.

11. L. C. Northcliffe, Ann. Rev. Nucl. Sci. 13, 67 (1963).

12. J. Lindhard and M. Scharff, Phys. Rev. 124, 128 (1961).

13. Yardley Beers, Introduction to the Theory of Errors, (Addison-Wesley Publishing Company Inc., Reading, Mass., 1962).

14. I. J. Taylor, F. de S. Barros, P. D. Forsyth, A. A. Jaffe and S. Ramavataram, Proc. Phys. Soc. 75, 772 (1960).

15. J. R. Patterson, J. M. Poate and E. W. Titterton, Proc. Phys. Soc. 85, 1085 (1965).

16. J. M. Blatt and V. F. Weisskopf, Theoretical Nuclear Physics, (John Wiley & Sons, New York, 1952).

17. J. P. Schiffer, Table of Charged Particle Penetrabilities (ANL 5739, June 1957).

18. F. Ajzenberg-Selove and T. Lauritsen, Nucl. Phys. 11, 1 (1959).

19. K. P. Swan, V. K. Rasmussen and F. R. Metzger, Phys. Rev. 121, 242 (1961).

20. E. C. Booth, B. Chasan and K. A. Wright, Nucl. Phys. 57, 463 (1964).

21. S. T. Butler, Nuclear Stripping Reactions, (John Wiley & Sons, New York, 1957).

22. N. K. Glendening, Ann. Rev. Nucl. Sci. 13, 191 (1963).

23. G. E. Owen and L. Mandansky, Phys. Rev. 105, 1766 (1957).

24. L. G. Earwaker, J. C. Jenkin and E. W. Titterton, Nucl. Phys. 46, 540 (1963).

25. W. Tobocman, Theory of Direct Nuclear Reactions, (Oxford University Press, London, 1961).

26. Leonard I. Schiff, Quantum Mechanics, (McGraw-Hill Book Company, Inc., New York, 1955).

27. A. B. Bhatia, K. Huang, R. Huby and H. C. Newns, Phil. Mag. 43, 485 (1952).

28. V. F. Weisskopf, Phys. Rev. 83, 1073 (1951).

29. D. H. Wilkinson, in Nuclear Spectroscopy, edited by F. Ajzenberg-Selove (Academic Press, Inc., New York, 1960), Part B, pp. 852-889.

30. G. Morpurgo, Phys. Rev. 110, 721 (1958).

31. E. K. Warburton, D. E. Alburger and D. H. Wilkinson, Phys. Rev. 132, 776 (1963).

32. E. K. Warburton, D. E. Alburger, A. Gallmann, P. Wagner and L. F. Chase, Jr., Phys. Rev. 133, B42 (1964).

33. M. G. Mayer and J. H. Jensen, Nuclear Shell Structure, (John Wiley & Sons, New York, 1955).

34. D. Kurath, Phys. Rev. 106, 975 (1957).

35. D. R. Inglis, Rev. Mod. Phys. 25, 390 (1953).

36. A. M. Lane, Proc. Phys. Soc. (London) A68, 189 (1955).

37. A. M. Lane and L. A. Radicati, Proc. Phys. Soc. (London) A67, 167 (1954).

38. D. Kurath, Phys. Rev. 101, 216 (1956).

39. E. K. Warburton and W. T. Pinkston, Phys. Rev. 118, 733 (1960).

40. D. A. Bromley, E. Almquist, A. E. Gove, A. E. Litherland, E. B. Paul and A. J. Fergusson, Phys. Rev. 105, 957 (1957).

41. J. P. Elliot, Phil. Mag. 1, 503 (1956).

42. V. M. Visscher and R. A. Ferrel, Phys. Rev. 107, 781 (1957).

43. R. S. Blake, D. J. Jacobs, J. O. Newton and J. P. Shapiro, Phys. Lett. 14, 74 (1965).

44. R. L. Heath, AEC Report IDO-15408 (1957).